

## Activation of the urotensin-II receptor by remdesivir induces cardiomyocyte dysfunction

Akiko Ogawa<sup>1,8</sup>, Seiya Ohira<sup>1,2,8</sup>, Yuri Kato<sup>3</sup>, Tatsuya Ikuta<sup>4</sup>, Shota Yanagida<sup>5,6</sup>, Xinya Mi<sup>3</sup>, Yukina Ishii<sup>3</sup>, Yasunari Kanda<sup>5</sup>, Motohiro Nishida<sup>3,7</sup>, Asuka Inoue<sup>4</sup> & Fan-Yan Wei<sup>1</sup>

Remdesivir is an antiviral drug used for COVID-19 treatment worldwide. Cardiovascular side effects have been associated with remdesivir; however, the underlying molecular mechanism remains unknown. Here, we performed a large-scale G-protein-coupled receptor screening in combination with structural modeling and found that remdesivir is a selective, partial agonist for urotensin-II receptor (UTS2R) through the  $G\alpha_{i/o}$ -dependent AKT/ERK axis. Functionally, remdesivir treatment induced prolonged field potential and APD<sub>90</sub> in human induced pluripotent stem cell (iPS)-derived cardiomyocytes and impaired contractility in both neonatal and adult cardiomyocytes, all of which mirror the clinical pathology. Importantly, remdesivir-mediated cardiac malfunctions were effectively attenuated by antagonizing UTS2R signaling. Finally, we characterized the effect of 110 single-nucleotide variants in *UTS2R* gene reported in genome database and found four missense variants that show gain-of-function effects in the receptor sensitivity to remdesivir. Collectively, our study illuminates a previously unknown mechanism underlying remdesivir-related cardiovascular events and that genetic variations of *UTS2R* gene can be a potential risk factor for cardiovascular events during remdesivir treatment, which collectively paves the way for a therapeutic opportunity to prevent such events in the future.

<sup>1</sup>Department of Modomics Biology and Medicine, Institute of Development, Aging and Cancer (IDAC), Tohoku University, Sendai, Miyagi 980-8575, Japan.

<sup>2</sup>Graduate School of Medicine, Tohoku University, Sendai, Miyagi 980-8575, Japan. <sup>3</sup>Department of Physiology, Graduate School of Pharmaceutical Sciences, Kyushu University, Fukuoka 812-8582, Japan. <sup>4</sup>Laboratory of Molecular & Cellular Biochemistry, Graduate School of Pharmaceutical Sciences, Tohoku University, 6-3, Aoba, Aramaki, Aoba-ku, Sendai, Miyagi 980-8578, Japan. <sup>5</sup>Division of Pharmacology, National Institute of Health Sciences, Kanagawa 210-9501, Japan.

<sup>6</sup>Division of Pharmaceutical Sciences, Graduate School of Medicine, Dentistry and Pharmaceutical Sciences, Okayama University, Okayama 700-8530, Japan.

<sup>7</sup>National Institute for Physiological Sciences and Exploratory Research Center on Life and Living Systems, National Institutes of Natural Sciences, Okazaki 444-8787, Japan. <sup>8</sup>These authors contributed equally: Akiko Ogawa, Seiya Ohira. ✉email: [nishida@phar.kyushu-u.ac.jp](mailto:nishida@phar.kyushu-u.ac.jp); [iaska@tohoku.ac.jp](mailto:iaska@tohoku.ac.jp); [fanyan.wei.d3@tohoku.ac.jp](mailto:fanyan.wei.d3@tohoku.ac.jp)

Nucleoside analogs have a long history in the field of drug design for antiviral treatment because nucleosides are used as building blocks for both DNA and RNA synthesis during viral replication<sup>1</sup>. The primary mechanism of nucleoside analogs' antiviral activities is attributed to the inhibition of the viral RNA-dependent RNA polymerase<sup>2</sup>. In response to the global pandemic of COVID-19, several nucleoside analogs, such as remdesivir, molnupiravir, and favipiravir, have been developed to treat the disease.

Remdesivir (GS-5734; Veklury) is a modified adenosine analog that contains a McGuigan prodrug moiety, including phenol and L-alanine ethylbutyl ester, which increases its lipophilicity and cell permeability<sup>3</sup>. Following intravenous administration, remdesivir is rapidly converted into the mono-nucleoside form (GS-441524) and is intracellularly metabolized by multiple host enzymes to its pharmacologically active triphosphate form, which, in turn, acts as a potent and selective inhibitor of the RNA-dependent RNA polymerase of multiple viruses<sup>4,5</sup>. Remdesivir was initially used for the treatment of Ebola virus<sup>6</sup> and has been approved for the treatment of Coronavirus Disease 2019 (COVID-19) amid the global pandemic. Remdesivir shortened the time to recovery in adults who were hospitalized with COVID-19 and had evidence of lower respiratory tract infection<sup>7</sup>. More recent data demonstrated a significant reduction in hospitalizations with a 3-day course of intravenous remdesivir<sup>8</sup>. Although remdesivir is generally well tolerated by most individuals, common adverse events for remdesivir have been reported, including rash, headache, nausea, diarrhea, and elevated transaminases<sup>7</sup>. Current guidelines for remdesivir suggest careful monitoring of liver function during treatment and recommend against its use in patients with renal dysfunction<sup>9</sup>. Additionally, cardiovascular events, including hypotension, bradycardia, QT prolongation, and T-wave abnormality, have been reported<sup>10–13</sup>. When administered intravenously, remdesivir shows broad tissue distribution, including to the heart<sup>14</sup>, but the precise molecular mechanism underlying the cardiovascular side-effects of remdesivir remains unclear.

Molnupiravir (EIDD-2801/MK-4482; Lagevrio) has been authorized for emergency use by the FDA under an Emergency Use Authorization for the treatment of mild-to-moderate COVID-19 in adults who are at high-risk for progression to severe COVID-19. Molnupiravir is an oral cytosine analog that contains an isopropylester prodrug of the  $\beta$ -D-N<sup>4</sup>-hydroxycytidine (NHC). The active form of NHC is a substrate of viral RNA-dependent RNA polymerase and impairs the fidelity of SARS-CoV-2 replication, provoking error catastrophe<sup>15</sup>. A clinical trial in nonhospitalized adults showed that early treatment with molnupiravir effectively reduced the risk of hospitalization or death in at-risk, unvaccinated adults with COVID-19<sup>16</sup>. In addition to molnupiravir, favipiravir (T-705; Avigan), which is an anti-influenza drug, has been under clinical trial for the treatment of COVID-19. Favipiravir is a nucleobase analog derived from pyrazine carboxamide (6-fluoro-3-hydroxy-2-pyrazinecarboxamide)<sup>17</sup>. The suggested modes of action of favipiravir comprise a mix of both chain termination and mutator events<sup>18</sup>. Several adverse events have been reported during the use of molnupiravir and favipiravir, including diarrhea, dizziness, and nausea for molnupiravir<sup>19</sup>, and hyperuricemia and increased alanine aminotransferase for favipiravir<sup>20</sup>. Importantly, unlike remdesivir, cardiovascular side effects have not been reported with the use of molnupiravir or favipiravir.

In addition to their function as building blocks for DNA/RNA synthesis, nucleotides/nucleosides can act as endogenous ligands for G-protein-coupled receptors (GPCR) and induce diverse pathophysiological responses<sup>21–25</sup>. Given the presence of nucleoside-mimicking structures in remdesivir, molnupiravir, and favipiravir, we hypothesized that these drugs might cause side

effects by directly activating GPCR. Here, we report that remdesivir, but not molnupiravir and favipiravir, is a selective ligand for the urotensin-II receptor (UTS2R) and causes cardiac dysfunction.

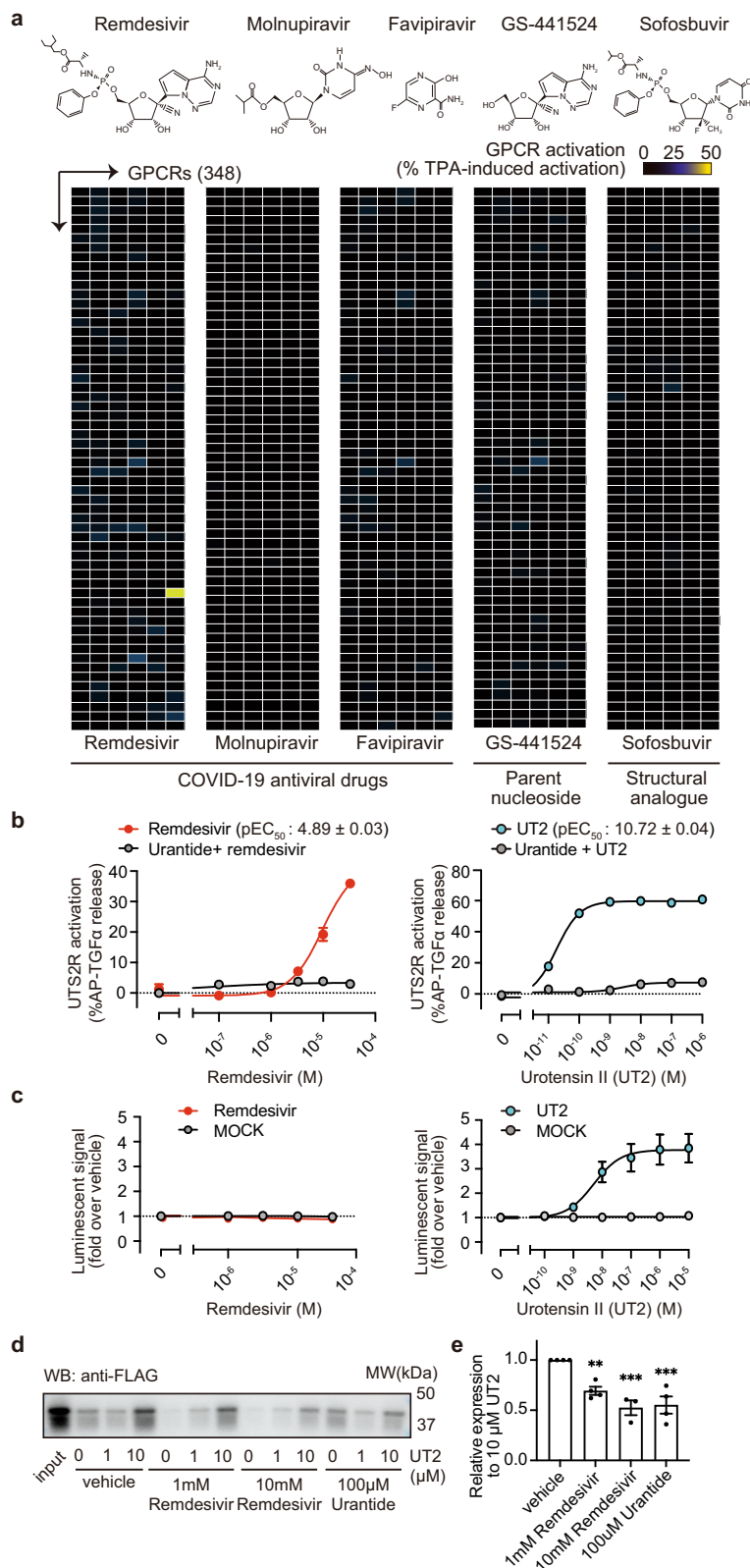
## Results

**Remdesivir is a selective, partial agonist of the urotensin-II receptor (UTS2R).** We screened anti-COVID-19 drugs, including remdesivir, molnupiravir, and favipiravir, against 348 GPCRs using an alkaline phosphatase-tagged transforming growth factor- $\alpha$  (AP-TGF $\alpha$ ) shedding assay<sup>26</sup>. We used chimeric G $\alpha$  subunit proteins for the initial screening to efficiently detect the receptor activation regardless of the type of G $\alpha$  subunit involved<sup>26</sup>. Among the three drugs, we discovered that remdesivir is a selective activator for the urotensin-II receptor (UTS2R) (Fig. 1a, Supplementary Fig. 1a, Supplementary Data 1). As remdesivir potently induced UTS2R response without any chimeric G $\alpha$  protein, the subsequent UTS2R analysis was performed without the exogenous addition of the chimeric G $\alpha$  protein. A concentration–response analysis revealed that the half-maximal effective concentration (pEC<sub>50</sub>) of remdesivir was  $4.89 \pm 0.03$  (EC<sub>50</sub> =  $13 \pm 0.9$   $\mu$ M, Fig. 1b left). It should be noted that both the potency and the efficacy of remdesivir ( $E_{\max} = 47 \pm 1.4$  %AP-TGF $\alpha$  release) toward UTS2R are lower than those of the endogenous peptidic ligand urotensin-II (UT2, pEC<sub>50</sub> =  $10.72 \pm 0.04$ ; EC<sub>50</sub> =  $21 \pm 2.1$  fM,  $E_{\max} = 59 \pm 0.70$  %AP-TGF $\alpha$  release, Fig. 1b right). Nevertheless, remdesivir administration at a clinical dosage is considered to be within the working range of agonistic effects because the maximum plasma concentration of remdesivir reaches 9.03  $\mu$ M after intravenous injection in healthy adults<sup>27</sup>. Interestingly, unlike UT2, remdesivir failed to induce a  $\beta$ -arrestin recruitment response (Fig. 1c, Supplementary Fig. 1b).

To evaluate whether remdesivir can directly interact with UTS2R, we performed a competitive binding assay. A previous study has shown that a synthetic UT2 peptide with an N-terminal biotin tag (biotin-UT2) can form stable binding with UTS2R<sup>28</sup>. Importantly, the binding was stable enough for biochemical pull-down of UTS2R using streptavidin resin. Taking advantage of the unique property of biotin-UT2 peptide, we performed a pull-down assay using membrane fraction of HEK293 cells expressing UTS2R in the presence or absence of remdesivir (Supplementary Fig. 1c). Among various types of magnetic beads that we tested, magnetic beads with hydrophobic coating showed the maximum pull-down efficacy with low non-specific binding (Supplementary Fig. 1d). Using the optimized protocol, we found that remdesivir and uranide significantly impaired biotin-UT2-mediated UTS2R pull-down (Fig. 1d, e, Supplementary Fig. 1e). These results suggest that remdesivir can directly interact with UTS2R, thereby interfering the biotin-UT2-UTS2R binding.

We further investigated whether the metabolites of remdesivir activate UTS2R. GS-441524 and GS-704277, the major and minor metabolites of remdesivir<sup>6,27</sup>, respectively, showed no effect on UTS2R activation (Fig. 1a, Supplementary Fig. 1a). To investigate whether the McGuigan prodrug moiety is responsible for remdesivir's UTS2R activation, we tested sofosbuvir (GS-7977), an FDA-approved McGuigan-class prodrug<sup>3</sup>, against UTS2R. However, sofosbuvir did not activate UTS2R (Fig. 1a, Supplementary Fig. 1a). These results suggest that both the McGuigan prodrug moiety and nucleoside base of remdesivir are required to activate the receptor.

**Molecular basis of UTS2R activation by remdesivir.** UTS2R belongs to the class A GPCR family<sup>29</sup> and consists of the canonical 7 transmembrane helices (TM), the amphipathic helix 8 at the C-terminus (H8), two antiparallel  $\beta$ -strands in the



extracellular loop 2, a relatively short N-terminal domain with two N-glycosylation sites, and a palmitoylation anchor at the C-terminal tail (Fig. 2a upper). Meanwhile, remdesivir is an analog of adenosine and a phosphoramidate prodrug of the McGuigan class (phenol and L-alanine ethylbutyl ester), which masks the anionic phosphate moiety on remdesivir, thus improving drug delivery. To further elucidate the molecular basis

for ligand-receptor binding, we performed in silico structural docking of UTS2R in the presence of remdesivir (Fig. 2a lower). Our analysis showed multiple amino acid residues in the orthosteric pocket that potentially stabilize binding to remdesivir. First, the cyano group of the nucleosugar of remdesivir forms a hydrogen bond to the UTS2R residue T304<sup>7.42×41</sup> (superscripts denote the generic GPCR numbering system<sup>30</sup>). Second, the

**Fig. 1 Identification of remdesivir as a selective agonist of urotensin-II receptor (UTS2R).** **a** Chemical structures of tested compounds and heatmaps showing the relative levels of GPCR activation as measured by the TGF $\alpha$ -shedding assay. The color scale represents the % GPCR activation compared to TPA (12-O-tetradecanoylphorbol 13-acetate)-mediated receptor activation, which induces the maximum TGF $\alpha$ -shedding response independently of GPCR. The yellow cell represents activation of UTS2R by remdesivir. The tested compounds' concentrations were 10  $\mu$ M for remdesivir, molnupiravir, GS-441524, and sofosbuvir, and 100  $\mu$ M for favipiravir ( $n = 3$ ). **b** TGF $\alpha$ -shedding response curves for UTS2R by remdesivir (left) and urotensin-II (UT2, right) in the presence or absence of urantide, a UTS2R antagonist (Data are shown as means  $\pm$  SEM,  $n = 3$ ). The half-maximal effective concentration (pEC $_{50}$ ) of remdesivir was  $4.89 \pm 0.03$  (EC $_{50} = 13 \mu$ M,  $E_{max} = 47 \pm 1.4$  %AP-TGF $\alpha$  release). The half-maximal effective concentration (pEC $_{50}$ ) of UT2 was  $10.72 \pm 0.04$  (EC $_{50} = 21$  fM,  $E_{max} = 59 \pm 0.70$  %AP-TGF $\alpha$  release). **c** Remdesivir (left)- or urotensin-II (UT2, right)-mediated  $\beta$ -arrestin 1 recruitment assay for UTS2R. Data are shown as means  $\pm$  SEM ( $n = 3$ ). **d, e** Competitive binding assay using biotin-UT2 peptide. The membrane fraction of HEK293 cells expressing FLAG-UTS2R (input) was incubated with biotin-UT2 in the presence or absence of remdesivir or urantide. FLAG-UTS2R was pulled down by streptavidin-coated magnetic beads (M280), and FLAG-UTS2R was detected by western blot. **d** Representative image of three independent trials was shown. **e** Band densitometry. \*\*\* $p < 0.001$  and \*\* $p < 0.01$  versus vehicle + 10  $\mu$ M UT2 group (one-way ANOVA followed by Dunnett's multiple comparisons test); means  $\pm$  SEM.

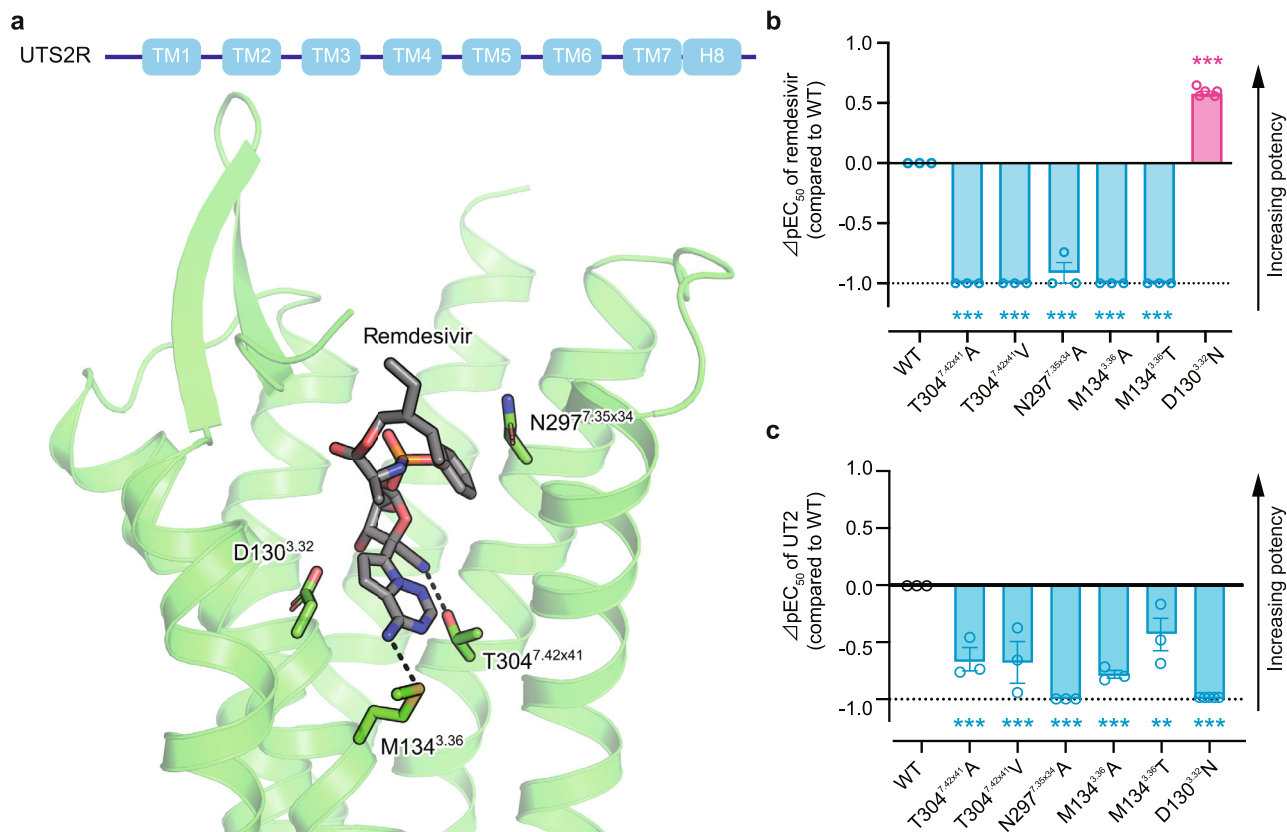


**Fig. 2 Docking simulation of UTS2R with remdesivir.** **a** Upper panel, Schematic of UTS2R; Lower panel, Docking model of UTS2R with remdesivir.

AlphaFold structure of human UTS2R is shown as green ribbons, omitting TM5 for clarity. Remdesivir and selected side chains of the receptor are shown as sticks and colored gray and green, respectively. Black dashed lines indicate hydrogen bonds. **b, c** Effects of the indicated mutations on remdesivir (**b**)- or UT2 (**c**)- mediated receptor activation. The y-axis ( $\Delta$ pEC $_{50}$  value) represents the relative activation potency of each mutant receptor compared to the WT receptor.  $\Delta$ pEC $_{50}$  value = pEC $_{50}$  mutant - pEC $_{50}$  WT. The  $\Delta$ pEC $_{50}$  cutoff value was set to -1, as indicated by dashed lines. EC $_{50}$  values were determined by the TGF $\alpha$ -shedding assay. \*\* $p < 0.01$ , \*\*\* $p < 0.001$  vs. WT by one-way ANOVA followed by Dunnett's multiple comparison test. Data are shown as means  $\pm$  SEM ( $n \geq 3$ ).

phenyl group of the McGuigan prodrug moiety of remdesivir is capped with N297<sup>7.35x34</sup>. Finally, the amino group of the nucleobase of remdesivir forms a hydrogen bond with M134<sup>3.36</sup> at the bottom of the pocket (NH...S hydrogen bond<sup>31</sup>).

To validate the docking model, we mutated these UTS2R residues (T304<sup>7.42x41</sup>, N297<sup>7.35x34</sup>, and M134<sup>3.36</sup>) to other amino acids and tested whether these mutations affect remdesivir-mediated UTS2R activation (Fig. 2b, c, Supplementary Fig. 2a, b). In line with the in silico simulation, mutation of the three residues almost completely abolished the activation potency of remdesivir to UTS2R, indicating that remdesivir needs to contact UTS2R at multiple residues to achieve stable binding. Both

nucleoside and McGuigan moiety are essential for receptor binding, with N297<sup>7.35x34</sup> interacting with the McGuigan moiety and M134<sup>3.36</sup> and T304<sup>7.42x41</sup> interacting with the nucleoside moiety. This structural observation explains why mutating a single amino acid strikingly reduces the remdesivir's activity towards UTS2R. This explanation is further supported by the result that UTS2R does not respond to any remdesivir metabolites, from which the McGuigan moiety is metabolically removed. In contrast, these mutations only partially reduced the UT2-mediated UTS2R activation. Meanwhile, contrary to these three residues, we found that D130<sup>3.32</sup> has an inhibitory effect on remdesivir-UTS2R binding. The D130<sup>3.32</sup>N mutation abolished

UT2-mediated UTS2R activation but significantly upregulated remdesivir-mediated receptor activation (Fig. 2b, c, Supplementary Fig. 2a, b). According to the docking model, the D130<sup>3.32</sup> residue is localized near the nucleobase moiety of remdesivir (Fig. 2a). We speculate that the negative charge of D130<sup>3.32</sup> residue may induce an electron repulsion effect<sup>32</sup>, leading to destabilization of the interaction between D130<sup>3.32</sup> residue and the nucleobase. These results demonstrate that remdesivir-mediated UTS2R activation is mediated by specific binding between UTS2R and its McGuigan prodrug moiety and nucleoside base, which differs from that of UTS2R and the endogenous ligand.

**Remdesivir-mediated UTS2R activation underlies drug-mediated cardiotoxicity.** To determine whether remdesivir-mediated UTS2R activation induces intracellular signaling transduction, we stimulated UTS2R-expressing HEK293 cells with remdesivir and examined the phosphorylation status of extracellular signal-regulated kinase (ERK)1/2. Application of remdesivir for up to 72 h evoked long-lasting and dose-dependent phosphorylation of ERK1/2 (Fig. 3a, Supplementary Fig. 3a). Importantly, remdesivir-mediated ERK phosphorylation was abolished by the UTS2R antagonist (Fig. 3a, Supplementary Fig. 3a). The response of ERK1/2 induced by remdesivir was similar to that induced by UT2 (Supplementary Fig. 3b).

UT2 and its receptor UTS2R are widely expressed in tissues, with relatively high expression in cardiovascular systems<sup>33</sup> (Supplementary Fig. 3c, d). Prompted by the cardiotoxic potential of remdesivir<sup>10–13</sup>, we assessed the impact of remdesivir on cardiomyocyte functions. We examined the effect of remdesivir on the field potential (FP) using human-induced pluripotent stem cell-derived cardiomyocytes (hiPSC-CMs)<sup>34</sup>, in which the expression level of *UTS2R* is comparable to that of the human heart (Supplementary Fig. 3e). The FP duration (FPD) correlates closely with the QT interval on an electrocardiogram (ECG)<sup>35</sup> (Fig. 3b left). Notably, the prolongation of the QT interval has been linked with the occurrence of severe and potentially fatal arrhythmias, and QT prolongation is the leading cause of drug-induced cardiovascular toxicity<sup>36</sup>. For the assessment of FPD, the use of a multielectrode array (MEA) platform is well-accepted for its ability to monitor the electrophysiology of cardiomyocytes at the cell population level (Fig. 3b right)<sup>35</sup>. An MEA analysis revealed that hiPSC-CMs treated with remdesivir showed a prolonged FPD of  $1.32 \pm 1.38\%$  at 24 h,  $5.60 \pm 1.60\%$  at 48 h, and  $15.57 \pm 3.49\%$  at 72 h, respectively. Notably, the prolongation was significantly suppressed by the UTS2R antagonist (Fig. 3c, d). Indeed, the application of UTS2R antagonist with remdesivir showed almost no FPD delay at 24 h ( $-1.71 \pm 1.60\%$ ) and 48 h ( $-0.61 \pm 0.11\%$ ), while the reversal effect was still significant but became partial at 72 h (Fig. 3d).

In addition to FPD, we evaluated QT prolongation by perforated patch-clamp and recorded spontaneous action potentials of hiPSC-CMs. We measured the APD<sub>90</sub> (action potential duration at 90% repolarization). Remdesivir significantly prolonged the APD<sub>90</sub> in hiPSC-CMs, and this prolongation was markedly attenuated by the administration of urantide (Fig. 3e). Thus, these results elucidate a previously unknown mechanism of the reported proarrhythmic risks of remdesivir<sup>11–13</sup>, which is at least partially dependent on UTS2R. Next, we assessed the effects of remdesivir on cardiac contractility. To this end, we used neonatal rat cardiomyocytes (NRCMs) and evaluated the contraction force. Under a constant pacing protocol, NRCMs with chronic remdesivir treatment showed reduced contractility, which was significantly attenuated by the UTS2R antagonist (Fig. 4a).

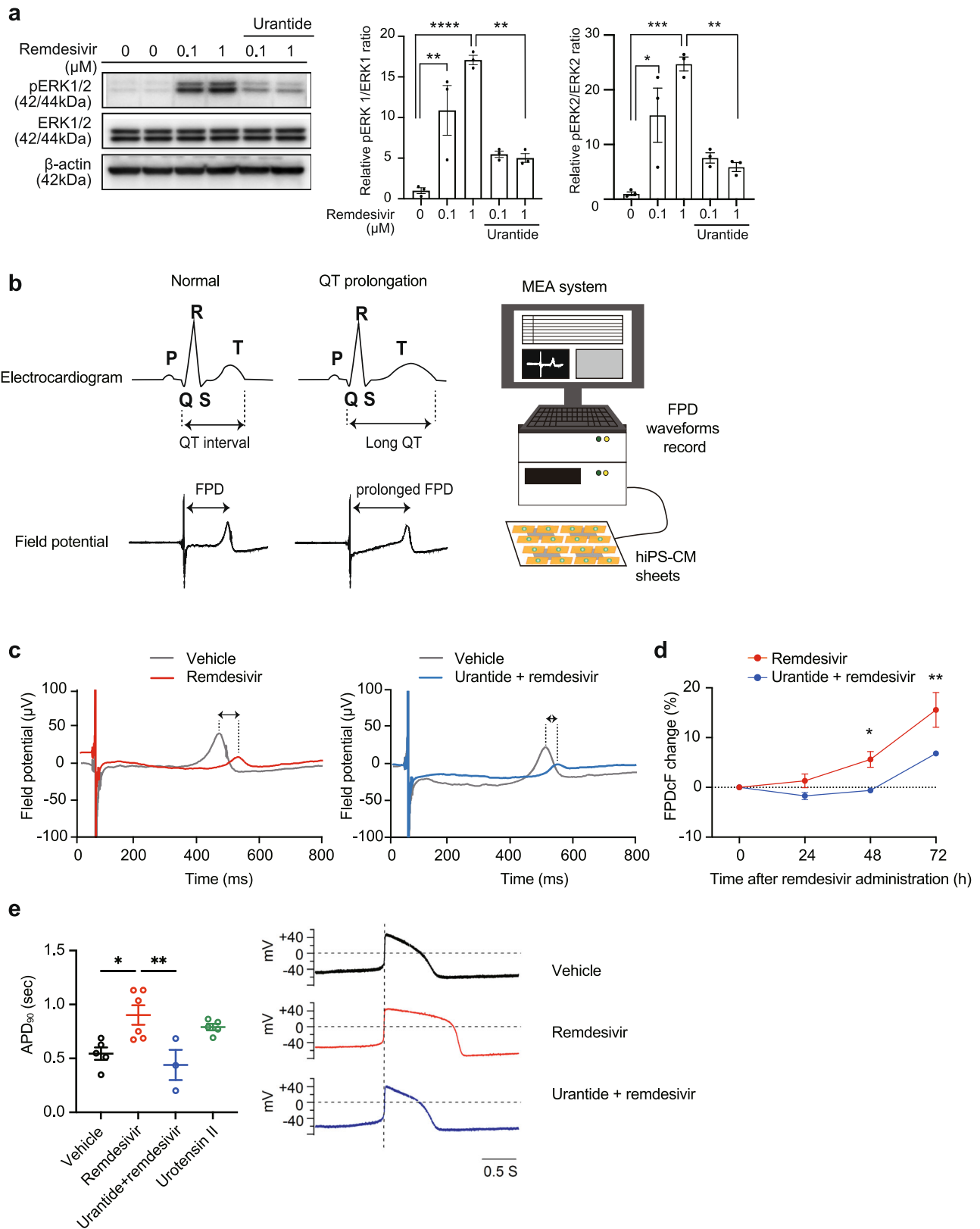
Heterotrimeric G proteins, including G $\alpha_s$ , G $\alpha_{i/o}$ , G $\alpha_{q/11}$ , and G $\alpha_{12/13}$ , are the downstream effectors of GPCRs. Among those, the G $\alpha_{i/o}$  family has been implicated in myocardial contractility and heart rate via the modulation of ion channels<sup>37</sup>. Since UTS2R is coupled to G $\alpha_{i/o}$  and G $\alpha_q$ <sup>29</sup>, we sought to determine which Ga protein is involved in the remdesivir-mediated decrease in myocardial contraction. G $\alpha_{i/o}$  inhibitor pertussis toxin (PTX), but not G $\alpha_{q/11}$  inhibitor YM-254890, completely blocked the effect of remdesivir and restored the peak contractions of NRCMs (Fig. 4b). A previous study demonstrated how activating G $\alpha_{i/o}$  in NRCMs leads to liberation of G $\beta\gamma$ , which intracellularly activates PI3K, leading to the activation of AKT and ERK1/2<sup>38</sup>. In line with this observation, G $\alpha_{i/o}$  inhibition reduced the remdesivir-induced phosphorylation of ERK1/2 and AKT (Fig. 4c, d). These results suggest that remdesivir reduces cardiomyocyte contractility through the G $\alpha_{i/o}$ -dependent AKT/ERK signal transduction pathway. Collectively, our results indicate that remdesivir itself can function as an exogenous ligand of UTS2R. Moreover, we identified the proarrhythmic and negative inotropic potential of remdesivir, both of which are UTS2R dependent.

Because neonatal cardiomyocytes are not terminally differentiated, we further investigated the effect of remdesivir on mature cardiomyocytes isolated from adult mouse hearts (Supplementary Fig. 3f). Contraction of cardiomyocytes was recorded under pacing conditions, and the degree of contraction was evaluated by morphological analysis. Similar to neonatal cardiomyocytes, remdesivir significantly impaired the contraction of adult cardiomyocytes (Fig. 4e, f).

A previous study suggested that remdesivir-related cardiotoxicity can be caused by mitochondrial dysfunction<sup>39</sup> since the active form of remdesivir shows an inhibitory effect toward mitochondrial RNA polymerase (mtRNAP) at a high dose<sup>40</sup>. However, treatment with remdesivir at 10  $\mu$ M, which is equivalent to the maximum plasma concentration following remdesivir administration in humans<sup>27</sup>, did not affect the steady-state levels of mitochondrial respiratory complex proteins (Supplementary Fig. 3g, h).

**Genetic effects of remdesivir-mediated UTS2R activation.** To understand the impact of genetic variance on the susceptibility to remdesivir–UTS2R signaling in humans, we extract single-nucleotide variant (SNV) information from a genome database that includes the 14KJPN Genome Reference Panel, which is a large-scale population-based genomic database constructed from the DNA sequence of 14,000 Japanese individuals<sup>41</sup>, followed by functional assay on receptor activation. A total of 2178 variants are reported in the *UTS2R* locus, of which 139 variants are missense variants (Supplementary Data 2). A considerable number of missense SNVs listed in the 14KJPN are also reported in the gnomAD database (<https://gnomad.broadinstitute.org>), which contains SNVs from broader ethnicities.

Accordingly, we generated 110 missense mutants corresponding to the human SNVs in the *UTS2R* gene. We excluded 29 missense mutations in the 5'-region of *UTS2R* as the confidence score for the structural prediction of the N-terminus was relatively low. Among the 110 missense SNVs, 44 SNVs showed a decrease in the sensitivity to remdesivir compared to the WT receptor ( $\Delta pEC_{50} < -0.3$ , which corresponds to over a twofold EC<sub>50</sub> increase compared to WT receptor; Fig. 5a upper panel). Meanwhile, 47 SNVs displayed a decreased sensitivity to UT2 compared to WT receptor, of which 18 SNVs overlapped with those that showed a decreased sensitivity to remdesivir (Fig. 5a lower panel, Supplementary Fig. 4a). Notably, we found four missense SNVs (G68<sup>1.49</sup>C, D130<sup>3.32</sup>G, V159<sup>34.54</sup>M, and A249<sup>ICL3</sup>G) that can increase the receptor sensitivity toward



remdesivir compared to the WT receptor ( $\Delta\text{pEC}_{50} > 0.3$ , which corresponds to a  $< 0.5$ -fold  $\text{EC}_{50}$  decrease compared to the WT receptor; Fig. 5a–c). Furthermore, among these four gain-of-function remdesivir-sensitive UTS2R SNVs, the G68<sup>1.48</sup>C and D130<sup>3.32</sup>G mutants conversely exhibited a decrease in the sensitivity toward UT2, while the V159<sup>34.54</sup>M and A249<sup>ICL3</sup>

mutants showed a moderate or insignificant increase in UT2 sensitivity ( $\Delta\text{pEC}_{50} < 0.3$ ; Fig. 5c, Supplementary Fig. 4a). Collectively, the results suggest that individuals with a G68<sup>1.49</sup>C, D130<sup>3.32</sup>G, V159<sup>34.54</sup>M, or A249<sup>ICL3</sup>G mutation in the UTS2R gene are sensitive to remdesivir, possibly making them more susceptible to UTS2R-mediated cardiotoxicity, although the allele

**Fig. 3 Cardiotoxic effects of remdesivir-mediated UTS2R activation.** **a** Serum-starved HEK293 cells overexpressing UTS2R were stimulated with the indicated concentrations of remdesivir for 5 min with or without urantide, a UTS2R antagonist, and the lysates subjected to western blotting analysis. ERK1 and ERK2 activation ratios (pERK1/ERK1 and pERK2/ERK2) were calculated with data normalized to the vehicle. \* $p < 0.05$ , \*\* $p < 0.01$ , \*\*\* $p < 0.001$ , \*\*\*\* $p < 0.0001$  by Tukey's multiple comparisons test. Data are represented as means  $\pm$  SEM ( $n = 3$ ). **b** Left, Temporal correlation between the field potential duration and the QT interval on the surface ECG. Right, Schematic of the multielectrode array (MEA) platform. **c** Representative field potential waveform in human induced pluripotent stem cell-derived cardiomyocytes (hiPSC-CMs) treated with 1  $\mu$ M remdesivir in the presence or absence of urantide for 72 h. **d** Effect of remdesivir and urantide on field potential prolongation in hiPSC-CMs. \* $p < 0.05$ , \*\* $p < 0.01$  by two-way ANOVA followed by Šidák's multiple comparisons tests. Data are represented as means  $\pm$  SEM ( $n = 3$ ). **e** Perforated patch-clamp to record spontaneous action potentials of hiPSC-CMs in current-clamp models. The hiPSC-CMs were treated with 10  $\mu$ M remdesivir in the presence or absence of 50  $\mu$ M urantide for 72 h. \* $p < 0.05$  and \*\* $p < 0.01$  by Tukey's multiple comparisons test. Data are represented as means  $\pm$  SEM ( $n \geq 3$ ).

frequencies of the gain-of-function variants are low (Supplementary Fig. 4b).

## Discussion

Following the completion of the Adaptive COVID-19 Treatment Trial 1 (ACTT-1)<sup>7</sup>, which demonstrated remdesivir's superiority over placebo for improving time to recovery in hospitalized COVID-19 patients, remdesivir has been one of the most commonly prescribed medications for patients hospitalized for COVID-19 infection. Importantly, the ACTT-1 investigators reported that 0.2% of patients receiving remdesivir, but not patients receiving placebo, showed arrhythmias (other than atrial fibrillation, supraventricular tachycardia, ventricular tachycardia, and ventricular fibrillation), although these cardiovascular effects were not considered as adverse effects. However, the percentage of patients experiencing arrhythmias could be underestimated since early clinical trials are insufficiently powered to detect uncommon adverse events<sup>42</sup>. Indeed, a large retrospective pharmacovigilance cohort study, which used medical records from more than 130 countries and 20 million patients, reported that cardiac arrest, bradycardia, and hypotension are associated with remdesivir use<sup>10</sup>. The elevation of plasma remdesivir concentration is associated with an increase in FP duration with decreased Na<sup>+</sup> peak amplitudes and spontaneous beating rates, which might potentially induce prolonged QT interval and torsade de point<sup>43,44</sup>. Importantly, the cardiac adverse effects appear to be directly caused by remdesivir, since they were reported to resolve within 24–48 h of discontinuing remdesivir<sup>45,46</sup>. To date, the precise mechanism underlying the remdesivir's cardiac side effects has remained unclear, with no means of predicting the populations susceptible to its cardiac side effects and no specific treatment for the cardiotoxicity. Therefore, there is a pressing need to understand how remdesivir induces cardiac dysfunction.

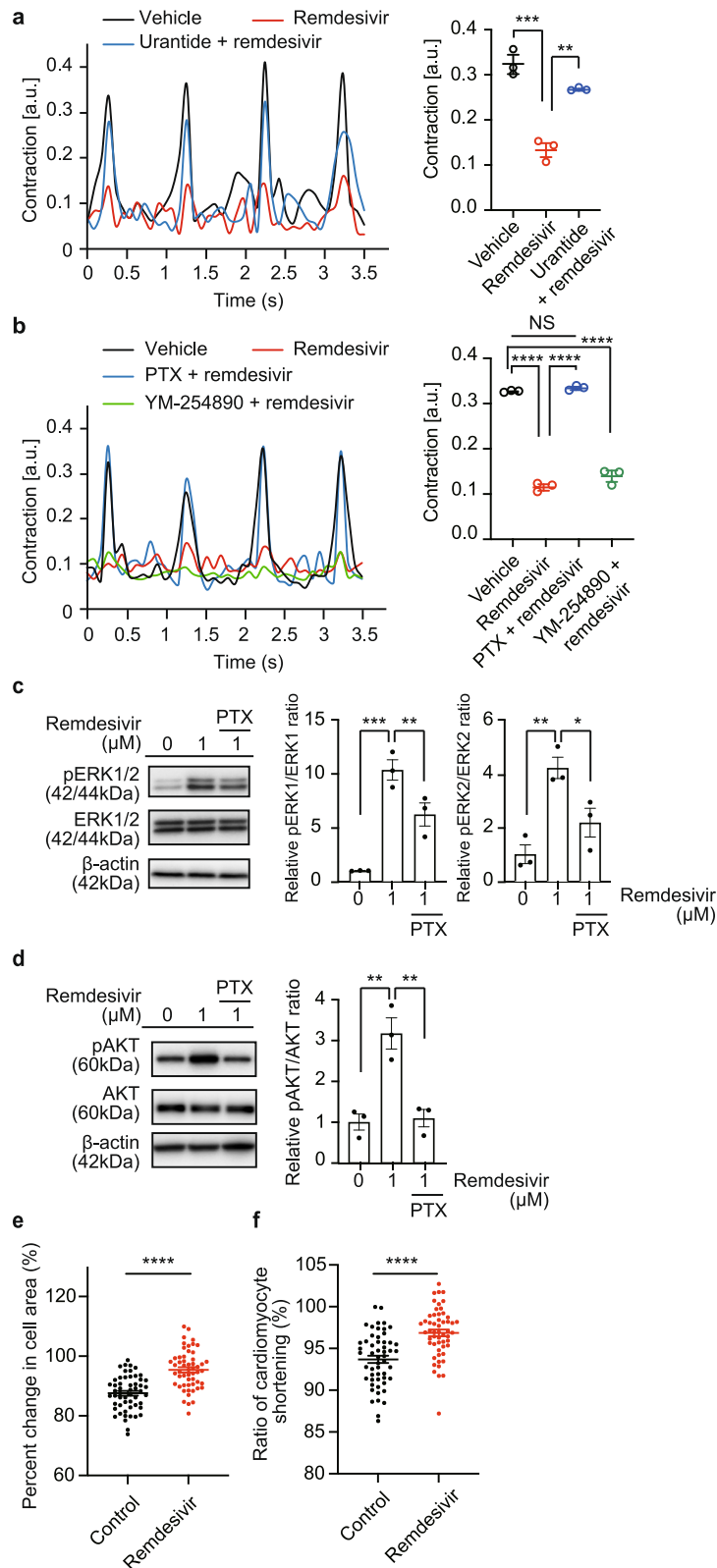
Using an unbiased and large-scale GPCR screening strategy, we identified that remdesivir, but not molnupiravir and favipiravir, can selectively activate UTS2R. The interaction between remdesivir and UTS2R was further supported by the competitive binding assay using the biotin-UT2 peptide. Interestingly, UTS2R is highly expressed in heart tissue, including cardiomyocytes. Activation of UTS2R by Urotensin-II (UT2), the endogenous ligand of UTS2R, has been implicated in cardiac dysfunction. For example, the plasma level of UT2 and expression level of UTS2R in cardiomyocytes are elevated in patients with end-stage congestive heart failure<sup>47</sup>. In line with these previous studies, we found that activation of UTS2R by remdesivir at a concentration of 1  $\mu$ M induced electrical abnormalities and contraction force impairment in cultured cardiomyocytes, both of which resemble the reported cardiac side effects in humans. Furthermore, these adverse effects were effectively blocked by antagonizing UTS2R or inhibiting its downstream signaling. Clinically, remdesivir is administered intravenously at a dose of 200 mg once, followed by 100 mg daily for a total of 5–10 days in adults and children  $\geq 40$  kg. The estimated peak plasma concentration of remdesivir is

9.03  $\mu$ M in healthy adults and can be higher in patients with renal or hepatic impairment because of its renal and biliary excretion<sup>48</sup>. Our results suggest that the clinical dosage of remdesivir is sufficient to activate UTS2R, and patients with renal or hepatic impairment may be at high risk for adverse events mediated through the remdesivir-UTS2R axis. Notably, our GPCR assay clearly showed that remdesivir has no effect on adenosine receptors, of which the activation can also impact cardiac functions. Thus, the activation of UTS2R is likely responsible for the cardiac side effects.

An important finding of this study is that SNVs in the coding region of UTS2R have large impacts on its response to remdesivir. This result is in line with previous studies that show SNVs in GPCR genes are associated with the pathophysiology of various diseases, including CV diseases, and affect therapeutic outcomes<sup>49</sup>. While 40% of SNVs in UTS2R (44/110) showed at least a twofold reduction in potency toward remdesivir compared to the WT receptor, and 56% (62/110) showed no remarkable change (within the range of an 0.5-fold to 2-fold change), we identified four gain-of-function SNVs that showed more than two-fold increase in response to remdesivir. Notably, D130<sup>3.32</sup>G was a variant at the same amino acid for which we identified a gain-of-function mutation (D130<sup>3.32</sup>N) using *in silico* modeling, indicating the importance of D130<sup>3.32</sup> residue in remdesivir recognition.

Activation of GPCR often induces recruitment of  $\beta$ -arrestin to the receptor, followed by receptor internalization to the intracellular compartment. This internalization terminates GPCR activation and promotes secondary signaling pathways<sup>50</sup>. Interestingly, unlike the endogenous ligand UT2, which effectively induces  $\beta$ -arrestin recruitment (Fig. 1c)<sup>51</sup>, remdesivir-mediated UTS2R activation did not induce  $\beta$ -arrestin recruitment. Thus, our results suggest that remdesivir is a G-protein-biased ligand (Fig. 1c, Supplementary Fig. 1b). Such biased activation of UTS2R by remdesivir may have an important impact on cardiac function in a way that allows prolonged activation of UTS2R without  $\beta$ -arrestin-mediated shutdown and thereby an exaggeration of downstream signaling and enhanced cardiotoxic effects. However, it is also conceivable that the modest potency of remdesivir could have hindered the detection of  $\beta$ -arrestin response. Further study using a new methodology for sensitive detection of the  $\beta$ -arrestin response is needed to evaluate the bias effect of remdesivir.

Upon ligand binding, GPCRs, including UTS2R, initiate conformational change that induces the activation of heterotrimeric G proteins and dissociation of G $\alpha$  and G $\beta\gamma$  subunit complexes. G $\alpha$  proteins include G $\alpha_s$ , G $\alpha_{i/o}$ , G $\alpha_{q/11}$ , and G $\alpha_{12/13}$  proteins, which are responsible for downstream signaling transduction. Members of the G $\alpha_{i/o}$  family are widely distributed, including in the cardiac system, where they are highly expressed and act to regulate myocardial contractility and heart rate via modulation of ion channels<sup>37</sup>. For example, resting heart rate is controlled by cholinergic signals mediated through muscarinic M2 G $\alpha_i$ -coupled receptors. These effects occur by inhibition of adenylyl cyclase (AC)



and by  $G\beta\gamma$ -inhibition of a potassium channel in the sinoatrial node. The transduction mechanism of UTS2R is the coupling and activation of  $G\alpha_{i/o}$  as well as  $G\alpha_q$ <sup>29</sup>, consistent with the UT2–UTS2R axis being implicated in CV regulation through complex signaling pathways, both physiologically and pathologically. Our results using NRCMs clearly showed that the remdesivir-mediated decrease in myocardial contraction is dependent on

$G\alpha_{i/o}$ , but not  $G\alpha_{q/11}$  (Fig. 4b). Since NRCMs resemble the phenotype of atrial myocytes<sup>52</sup>, the decrease in myocardial contractility under constant pacing by remdesivir indicates impairment of calcium handling<sup>53</sup>, which is consistent with the slowing of the heart rate, a distinctive cardiovascular side effect of remdesivir<sup>10</sup>. Additionally, we showed that remdesivir significantly impaired the contractility of adult cardiomyocytes (Fig. 4e, f).

**Fig. 4 Cardiotoxic effects of remdesivir-mediated UTS2R activation.** **a, b** Left, Representative waveform of contractility under pacing in neonatal rat cardiomyocytes (NRCMs) by 1  $\mu$ M remdesivir with or without **a** urantide or **b** pertussis toxin (PTX), a  $G\alpha_{i/o}$  inhibitor, and YM-254890, a  $G\alpha_{q/11}$  inhibitor, at 48 h. Right, the effect of remdesivir with **a** urantide or **b** PTX and YM-254890 on contractility under pacing in NRCMs.  $**p < 0.01$ ,  $***p < 0.001$ ,  $****p < 0.0001$  by Tukey's multiple comparisons test. Data are represented as means  $\pm$  SEM ( $n = 3$ ). **c, d** Representative western blot for phosphorylation of **c** ERK1/2 and **d** protein kinase B (AKT). Serum-starved HEK293 cells overexpressing UTS2R were stimulated with the indicated concentrations of remdesivir for 48 h. For  $G_{i/o}$  protein inhibition, cells were incubated with PTX for at least 18 h at 150 ng/mL. ERK1, ERK2, and AKT activation ratios were calculated with data normalized to the vehicle.  $*p < 0.05$ ,  $**p < 0.01$ ,  $***p < 0.001$  by Tukey's multiple comparisons test. Data are shown as means  $\pm$  SEM ( $n = 3$ ). **e, f** The effects of remdesivir on the contractility of adult mouse cardiomyocytes. Isolated adult mouse cardiomyocytes were treated with remdesivir (10  $\mu$ M) for 30 min, and the percentile change in cell area (**e**) and the ratio of cardiomyocyte shortening (**f**) was measured during electrical pacing.  $****p < 0.001$  by unpaired  $t$ -test. Data are shown as means  $\pm$  SEM (a total of 54 cells from 3 mice).

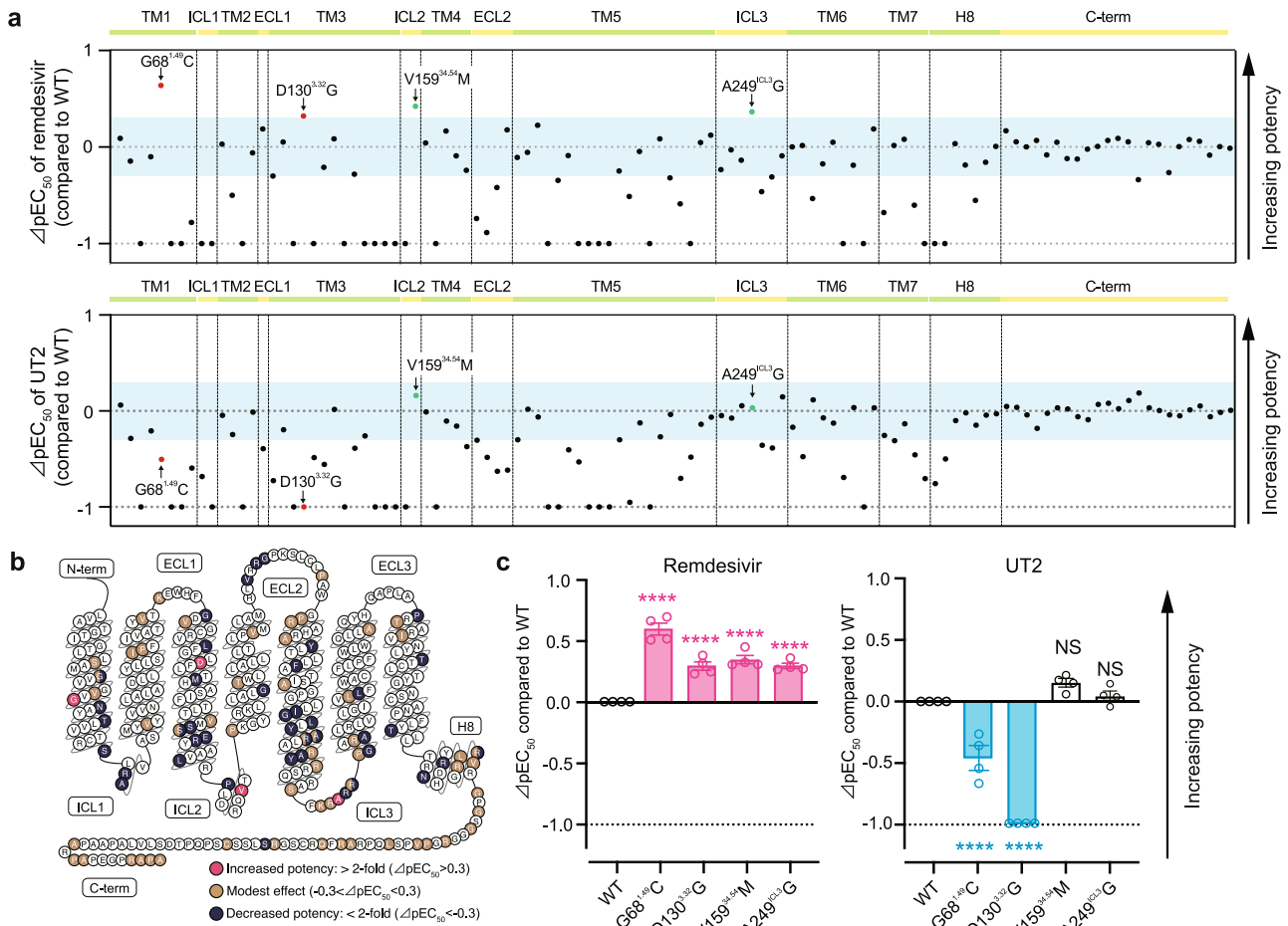


**Fig. 5 Genetic effects of remdesivir-mediated UTS2R activation.** **a** Effects of 110 missense SNVs from the *UTS2R* gene on (upper panel) remdesivir-mediated and (lower panel) UT2-mediated receptor activation, measured by the TGF $\alpha$ -shedding assay. The y-axis ( $\Delta pEC_{50}$  value) represents the relative activation potency of each mutant receptor compared to the WT receptor. The  $\Delta pEC_{50}$  cutoff value was set to  $-1$ , as indicated by dashed lines. Light blue bands represent the range of  $-0.3 < \Delta pEC_{50} < 0.3$ , which corresponds to the range of an 0.5-fold to 2-fold (less than 2-fold) change in the  $EC_{50}$  of the mutant receptor compared to the WT receptor. All experiments were performed in triplicate, and the data are expressed as the means. **b** Snake plot diagram of UTS2R showing locations of mutations and their effects on the potency of remdesivir (modified from [www.gpcrcdb.org](http://www.gpcrcdb.org)). **c** Effects of the selected mutations on (left) remdesivir-mediated and (right) UT2-mediated receptor activation.  $EC_{50}$  values are determined by the TGF $\alpha$ -shedding assay. "ns"  $p > 0.05$ , and  $****p < 0.0001$  vs. WT by one-way ANOVA followed by Dunnett's multiple comparisons tests. Data are shown as means  $\pm$  SEM ( $n \geq 3$ ).

Despite the discovery that remdesivir can activate UTS2R and cause cardiotoxicity, the lack of clinical evidence is a major limitation of this study. Yet, as the allele frequencies of the gain-of-function variants are low, (Supplementary Fig. 4b) and usage of remdesivir is expected to decline due to the recent prevalence of the Omicron COVID-19 variant with its milder symptoms, a large-scale clinical study on the association between remdesivir sensitivity and genomic variance is challenging to execute. Additionally, we have not determined the precise molecular mechanisms that induce the UTS2R-dependent proarrhythmic

risk of remdesivir. Possible explanations are the impaired regulation of gene expression or trafficking of ERG potassium channels, which are essential for electrical activity in the heart<sup>54</sup>. Alternatively, the chronic and cumulative cardiotoxic effects of the remdesivir–UTS2R axis are consistent with a downstream impact on translation and transcription. Although we do not exclude the possibility that remdesivir might affect mitochondrial metabolism through UTS2R signal transduction (Supplementary Fig. 3f), the current data suggest that the remdesivir–UTS2R axis is the major off-target of remdesivir.

In conclusion, to our knowledge, this is the first report showing that remdesivir is a selective agonist of UTS2R and that remdesivir-mediated UTS2R activation underlies drug-mediated cardiotoxicity. Furthermore, we discovered that specific SNVs in UTS2R can increase the sensitivity to remdesivir. Thus, this study provides mechanistic insights into remdesivir-mediated cardiac side effects and the therapeutic opportunity to prevent aversive events in the future.

## Methods

**Study design.** The overall goal of this study was to explore the molecular mechanisms of remdesivir-related cardiotoxicity in anti-COVID-19 therapy. We first performed the GPCR screening using major anti-COVID-19 drugs as ligands ( $n = 3$  per GPCR). We validated the results of GPCR screening by concentration-response analysis and determined the  $EC_{50}$  and  $E_{max}$  values of remdesivir against UTS2R ( $n = 16$ ). We also performed docking simulation using AlphaFold and determined the key amino acid residues that were essential for remdesivir-UTS2R binding, as demonstrated by a mutagenesis study ( $n \geq 3$ ). We next examined the cardiotoxic potential of remdesivir. Using hiPS-derived cardiomyocytes, we found that the proarrhythmic risk of remdesivir is largely mediated by UTS2R ( $n = 3$ ). Moreover, using NRCMs, we showed that the decrease in contraction force by remdesivir is mediated by the UTS2R- $G\alpha_{i/o}$  axis ( $n = 3$ ). Finally, the effects of SNVs in the UTS2R gene on remdesivir-mediated receptor activation were evaluated using a GPCR assay ( $n = 3$  per SNV).

**Chemicals.** Remdesivir (GS-5734), GS-441524, and sofosbuvir (GS-7977) were purchased from Selleck Chemicals. Favipiravir was purchased from Tokyo Chemical Industry. Fibronectin was purchased from Sigma-Aldrich. All other reagents were of analytical grade and obtained from commercial sources.

**SNV in the human UTS2R coding region.** To search for SNVs in UTS2R, we used a public database of 14,000 healthy Japanese individuals, called 14KJPN, released by Tohoku University's Tohoku Medical Megabank Organization (ToMMO, <https://jmorp.megabank.tohoku.ac.jp/>)<sup>41</sup>, which covers variant frequency data.

**TGF $\alpha$ -shedding assay-based GPCR screening.** To measure the activation of the GPCR, a transforming growth factor- $\alpha$  (TGF $\alpha$ ) shedding assay was performed<sup>26</sup>. Briefly, HEK293A cells were seeded in a 12-well culture plate. A total of 348 pCAG plasmids encoding an untagged GPCR, including the UTS2R construct, were prepared (Supplementary Data 1). The UTS2R mutants, including 110 missense mutants corresponding to the human SNVs in the UTS2R gene, were generated by introducing single-point mutations using a KOD-Plus-Mutagenesis kit. Cells were transfected using a polyethylenimine (PEI) reagent (2.5  $\mu$ l of 1 mg/ml per well hereafter; Polysciences) with these UTS2R plasmids (100 ng per well hereafter), together with the plasmids encoding alkaline phosphatase (AP)-tagged TGF $\alpha$  (AP-TGF $\alpha$ ; 250 ng). UTS2R activation assays were performed with endogenous G protein unless otherwise specified. Chimeric G $\alpha$  subunit proteins (mixture of  $G\alpha_{q/11}$ ,  $G\alpha_{q/13}$ ,  $G\alpha_{q/15}$ ,  $G\alpha_{q/17}$ ,  $G\alpha_{q/19}$ ,  $G\alpha_{q/20}$ ,  $G\alpha_{q/21}$ ,  $G\alpha_{q/22}$ ,  $G\alpha_{q/23}$ ,  $G\alpha_{q/24}$ ,  $G\alpha_{q/25}$ ,  $G\alpha_{q/26}$ ,  $G\alpha_{q/27}$ ,  $G\alpha_{q/28}$ ,  $G\alpha_{q/29}$ ,  $G\alpha_{q/30}$ ,  $G\alpha_{q/31}$ ,  $G\alpha_{q/32}$ ,  $G\alpha_{q/33}$ ,  $G\alpha_{q/34}$ ,  $G\alpha_{q/35}$ ,  $G\alpha_{q/36}$ ,  $G\alpha_{q/37}$ ,  $G\alpha_{q/38}$ ,  $G\alpha_{q/39}$ ,  $G\alpha_{q/40}$ ,  $G\alpha_{q/41}$ ,  $G\alpha_{q/42}$ ,  $G\alpha_{q/43}$ ,  $G\alpha_{q/44}$ ,  $G\alpha_{q/45}$ ,  $G\alpha_{q/46}$ ,  $G\alpha_{q/47}$ ,  $G\alpha_{q/48}$ ,  $G\alpha_{q/49}$ ,  $G\alpha_{q/50}$ ,  $G\alpha_{q/51}$ ,  $G\alpha_{q/52}$ ,  $G\alpha_{q/53}$ ,  $G\alpha_{q/54}$ ,  $G\alpha_{q/55}$ ,  $G\alpha_{q/56}$ ,  $G\alpha_{q/57}$ ,  $G\alpha_{q/58}$ ,  $G\alpha_{q/59}$ ,  $G\alpha_{q/60}$ ,  $G\alpha_{q/61}$ ,  $G\alpha_{q/62}$ ,  $G\alpha_{q/63}$ ,  $G\alpha_{q/64}$ ,  $G\alpha_{q/65}$ ,  $G\alpha_{q/66}$ ,  $G\alpha_{q/67}$ ,  $G\alpha_{q/68}$ ,  $G\alpha_{q/69}$ ,  $G\alpha_{q/70}$ ,  $G\alpha_{q/71}$ ,  $G\alpha_{q/72}$ ,  $G\alpha_{q/73}$ ,  $G\alpha_{q/74}$ ,  $G\alpha_{q/75}$ ,  $G\alpha_{q/76}$ ,  $G\alpha_{q/77}$ ,  $G\alpha_{q/78}$ ,  $G\alpha_{q/79}$ ,  $G\alpha_{q/80}$ ,  $G\alpha_{q/81}$ ,  $G\alpha_{q/82}$ ,  $G\alpha_{q/83}$ ,  $G\alpha_{q/84}$ ,  $G\alpha_{q/85}$ ,  $G\alpha_{q/86}$ ,  $G\alpha_{q/87}$ ,  $G\alpha_{q/88}$ ,  $G\alpha_{q/89}$ ,  $G\alpha_{q/90}$ ,  $G\alpha_{q/91}$ ,  $G\alpha_{q/92}$ ,  $G\alpha_{q/93}$ ,  $G\alpha_{q/94}$ ,  $G\alpha_{q/95}$ ,  $G\alpha_{q/96}$ ,  $G\alpha_{q/97}$ ,  $G\alpha_{q/98}$ ,  $G\alpha_{q/99}$ ,  $G\alpha_{q/100}$ ,  $G\alpha_{q/101}$ ,  $G\alpha_{q/102}$ ,  $G\alpha_{q/103}$ ,  $G\alpha_{q/104}$ ,  $G\alpha_{q/105}$ ,  $G\alpha_{q/106}$ ,  $G\alpha_{q/107}$ ,  $G\alpha_{q/108}$ ,  $G\alpha_{q/109}$ ,  $G\alpha_{q/110}$ ,  $G\alpha_{q/111}$ ,  $G\alpha_{q/112}$ ,  $G\alpha_{q/113}$ ,  $G\alpha_{q/114}$ ,  $G\alpha_{q/115}$ ,  $G\alpha_{q/116}$ ,  $G\alpha_{q/117}$ ,  $G\alpha_{q/118}$ ,  $G\alpha_{q/119}$ ,  $G\alpha_{q/120}$ ,  $G\alpha_{q/121}$ ,  $G\alpha_{q/122}$ ,  $G\alpha_{q/123}$ ,  $G\alpha_{q/124}$ ,  $G\alpha_{q/125}$ ,  $G\alpha_{q/126}$ ,  $G\alpha_{q/127}$ ,  $G\alpha_{q/128}$ ,  $G\alpha_{q/129}$ ,  $G\alpha_{q/130}$ ,  $G\alpha_{q/131}$ ,  $G\alpha_{q/132}$ ,  $G\alpha_{q/133}$ ,  $G\alpha_{q/134}$ ,  $G\alpha_{q/135}$ ,  $G\alpha_{q/136}$ ,  $G\alpha_{q/137}$ ,  $G\alpha_{q/138}$ ,  $G\alpha_{q/139}$ ,  $G\alpha_{q/140}$ ,  $G\alpha_{q/141}$ ,  $G\alpha_{q/142}$ ,  $G\alpha_{q/143}$ ,  $G\alpha_{q/144}$ ,  $G\alpha_{q/145}$ ,  $G\alpha_{q/146}$ ,  $G\alpha_{q/147}$ ,  $G\alpha_{q/148}$ ,  $G\alpha_{q/149}$ ,  $G\alpha_{q/150}$ ,  $G\alpha_{q/151}$ ,  $G\alpha_{q/152}$ ,  $G\alpha_{q/153}$ ,  $G\alpha_{q/154}$ ,  $G\alpha_{q/155}$ ,  $G\alpha_{q/156}$ ,  $G\alpha_{q/157}$ ,  $G\alpha_{q/158}$ ,  $G\alpha_{q/159}$ ,  $G\alpha_{q/160}$ ,  $G\alpha_{q/161}$ ,  $G\alpha_{q/162}$ ,  $G\alpha_{q/163}$ ,  $G\alpha_{q/164}$ ,  $G\alpha_{q/165}$ ,  $G\alpha_{q/166}$ ,  $G\alpha_{q/167}$ ,  $G\alpha_{q/168}$ ,  $G\alpha_{q/169}$ ,  $G\alpha_{q/170}$ ,  $G\alpha_{q/171}$ ,  $G\alpha_{q/172}$ ,  $G\alpha_{q/173}$ ,  $G\alpha_{q/174}$ ,  $G\alpha_{q/175}$ ,  $G\alpha_{q/176}$ ,  $G\alpha_{q/177}$ ,  $G\alpha_{q/178}$ ,  $G\alpha_{q/179}$ ,  $G\alpha_{q/180}$ ,  $G\alpha_{q/181}$ ,  $G\alpha_{q/182}$ ,  $G\alpha_{q/183}$ ,  $G\alpha_{q/184}$ ,  $G\alpha_{q/185}$ ,  $G\alpha_{q/186}$ ,  $G\alpha_{q/187}$ ,  $G\alpha_{q/188}$ ,  $G\alpha_{q/189}$ ,  $G\alpha_{q/190}$ ,  $G\alpha_{q/191}$ ,  $G\alpha_{q/192}$ ,  $G\alpha_{q/193}$ ,  $G\alpha_{q/194}$ ,  $G\alpha_{q/195}$ ,  $G\alpha_{q/196}$ ,  $G\alpha_{q/197}$ ,  $G\alpha_{q/198}$ ,  $G\alpha_{q/199}$ ,  $G\alpha_{q/200}$ ,  $G\alpha_{q/201}$ ,  $G\alpha_{q/202}$ ,  $G\alpha_{q/203}$ ,  $G\alpha_{q/204}$ ,  $G\alpha_{q/205}$ ,  $G\alpha_{q/206}$ ,  $G\alpha_{q/207}$ ,  $G\alpha_{q/208}$ ,  $G\alpha_{q/209}$ ,  $G\alpha_{q/210}$ ,  $G\alpha_{q/211}$ ,  $G\alpha_{q/212}$ ,  $G\alpha_{q/213}$ ,  $G\alpha_{q/214}$ ,  $G\alpha_{q/215}$ ,  $G\alpha_{q/216}$ ,  $G\alpha_{q/217}$ ,  $G\alpha_{q/218}$ ,  $G\alpha_{q/219}$ ,  $G\alpha_{q/220}$ ,  $G\alpha_{q/221}$ ,  $G\alpha_{q/222}$ ,  $G\alpha_{q/223}$ ,  $G\alpha_{q/224}$ ,  $G\alpha_{q/225}$ ,  $G\alpha_{q/226}$ ,  $G\alpha_{q/227}$ ,  $G\alpha_{q/228}$ ,  $G\alpha_{q/229}$ ,  $G\alpha_{q/230}$ ,  $G\alpha_{q/231}$ ,  $G\alpha_{q/232}$ ,  $G\alpha_{q/233}$ ,  $G\alpha_{q/234}$ ,  $G\alpha_{q/235}$ ,  $G\alpha_{q/236}$ ,  $G\alpha_{q/237}$ ,  $G\alpha_{q/238}$ ,  $G\alpha_{q/239}$ ,  $G\alpha_{q/240}$ ,  $G\alpha_{q/241}$ ,  $G\alpha_{q/242}$ ,  $G\alpha_{q/243}$ ,  $G\alpha_{q/244}$ ,  $G\alpha_{q/245}$ ,  $G\alpha_{q/246}$ ,  $G\alpha_{q/247}$ ,  $G\alpha_{q/248}$ ,  $G\alpha_{q/249}$ ,  $G\alpha_{q/250}$ ,  $G\alpha_{q/251}$ ,  $G\alpha_{q/252}$ ,  $G\alpha_{q/253}$ ,  $G\alpha_{q/254}$ ,  $G\alpha_{q/255}$ ,  $G\alpha_{q/256}$ ,  $G\alpha_{q/257}$ ,  $G\alpha_{q/258}$ ,  $G\alpha_{q/259}$ ,  $G\alpha_{q/260}$ ,  $G\alpha_{q/261}$ ,  $G\alpha_{q/262}$ ,  $G\alpha_{q/263}$ ,  $G\alpha_{q/264}$ ,  $G\alpha_{q/265}$ ,  $G\alpha_{q/266}$ ,  $G\alpha_{q/267}$ ,  $G\alpha_{q/268}$ ,  $G\alpha_{q/269}$ ,  $G\alpha_{q/270}$ ,  $G\alpha_{q/271}$ ,  $G\alpha_{q/272}$ ,  $G\alpha_{q/273}$ ,  $G\alpha_{q/274}$ ,  $G\alpha_{q/275}$ ,  $G\alpha_{q/276}$ ,  $G\alpha_{q/277}$ ,  $G\alpha_{q/278}$ ,  $G\alpha_{q/279}$ ,  $G\alpha_{q/280}$ ,  $G\alpha_{q/281}$ ,  $G\alpha_{q/282}$ ,  $G\alpha_{q/283}$ ,  $G\alpha_{q/284}$ ,  $G\alpha_{q/285}$ ,  $G\alpha_{q/286}$ ,  $G\alpha_{q/287}$ ,  $G\alpha_{q/288}$ ,  $G\alpha_{q/289}$ ,  $G\alpha_{q/290}$ ,  $G\alpha_{q/291}$ ,  $G\alpha_{q/292}$ ,  $G\alpha_{q/293}$ ,  $G\alpha_{q/294}$ ,  $G\alpha_{q/295}$ ,  $G\alpha_{q/296}$ ,  $G\alpha_{q/297}$ ,  $G\alpha_{q/298}$ ,  $G\alpha_{q/299}$ ,  $G\alpha_{q/300}$ ,  $G\alpha_{q/301}$ ,  $G\alpha_{q/302}$ ,  $G\alpha_{q/303}$ ,  $G\alpha_{q/304}$ ,  $G\alpha_{q/305}$ ,  $G\alpha_{q/306}$ ,  $G\alpha_{q/307}$ ,  $G\alpha_{q/308}$ ,  $G\alpha_{q/309}$ ,  $G\alpha_{q/310}$ ,  $G\alpha_{q/311}$ ,  $G\alpha_{q/312}$ ,  $G\alpha_{q/313}$ ,  $G\alpha_{q/314}$ ,  $G\alpha_{q/315}$ ,  $G\alpha_{q/316}$ ,  $G\alpha_{q/317}$ ,  $G\alpha_{q/318}$ ,  $G\alpha_{q/319}$ ,  $G\alpha_{q/320}$ ,  $G\alpha_{q/321}$ ,  $G\alpha_{q/322}$ ,  $G\alpha_{q/323}$ ,  $G\alpha_{q/324}$ ,  $G\alpha_{q/325}$ ,  $G\alpha_{q/326}$ ,  $G\alpha_{q/327}$ ,  $G\alpha_{q/328}$ ,  $G\alpha_{q/329}$ ,  $G\alpha_{q/330}$ ,  $G\alpha_{q/331}$ ,  $G\alpha_{q/332}$ ,  $G\alpha_{q/333}$ ,  $G\alpha_{q/334}$ ,  $G\alpha_{q/335}$ ,  $G\alpha_{q/336}$ ,  $G\alpha_{q/337}$ ,  $G\alpha_{q/338}$ ,  $G\alpha_{q/339}$ ,  $G\alpha_{q/340}$ ,  $G\alpha_{q/341}$ ,  $G\alpha_{q/342}$ ,  $G\alpha_{q/343}$ ,  $G\alpha_{q/344}$ ,  $G\alpha_{q/345}$ ,  $G\alpha_{q/346}$ ,  $G\alpha_{q/347}$ ,  $G\alpha_{q/348}$ ,  $G\alpha_{q/349}$ ,  $G\alpha_{q/350}$ ,  $G\alpha_{q/351}$ ,  $G\alpha_{q/352}$ ,  $G\alpha_{q/353}$ ,  $G\alpha_{q/354}$ ,  $G\alpha_{q/355}$ ,  $G\alpha_{q/356}$ ,  $G\alpha_{q/357}$ ,  $G\alpha_{q/358}$ ,  $G\alpha_{q/359}$ ,  $G\alpha_{q/360}$ ,  $G\alpha_{q/361}$ ,  $G\alpha_{q/362}$ ,  $G\alpha_{q/363}$ ,  $G\alpha_{q/364}$ ,  $G\alpha_{q/365}$ ,  $G\alpha_{q/366}$ ,  $G\alpha_{q/367}$ ,  $G\alpha_{q/368}$ ,  $G\alpha_{q/369}$ ,  $G\alpha_{q/370}$ ,  $G\alpha_{q/371}$ ,  $G\alpha_{q/372}$ ,  $G\alpha_{q/373}$ ,  $G\alpha_{q/374}$ ,  $G\alpha_{q/375}$ ,  $G\alpha_{q/376}$ ,  $G\alpha_{q/377}$ ,  $G\alpha_{q/378}$ ,  $G\alpha_{q/379}$ ,  $G\alpha_{q/380}$ ,  $G\alpha_{q/381}$ ,  $G\alpha_{q/382}$ ,  $G\alpha_{q/383}$ ,  $G\alpha_{q/384}$ ,  $G\alpha_{q/385}$ ,  $G\alpha_{q/386}$ ,  $G\alpha_{q/387}$ ,  $G\alpha_{q/388}$ ,  $G\alpha_{q/389}$ ,  $G\alpha_{q/390}$ ,  $G\alpha_{q/391}$ ,  $G\alpha_{q/392}$ ,  $G\alpha_{q/393}$ ,  $G\alpha_{q/394}$ ,  $G\alpha_{q/395}$ ,  $G\alpha_{q/396}$ ,  $G\alpha_{q/397}$ ,  $G\alpha_{q/398}$ ,  $G\alpha_{q/399}$ ,  $G\alpha_{q/400}$ ,  $G\alpha_{q/401}$ ,  $G\alpha_{q/402}$ ,  $G\alpha_{q/403}$ ,  $G\alpha_{q/404}$ ,  $G\alpha_{q/405}$ ,  $G\alpha_{q/406}$ ,  $G\alpha_{q/407}$ ,  $G\alpha_{q/408}$ ,  $G\alpha_{q/409}$ ,  $G\alpha_{q/410}$ ,  $G\alpha_{q/411}$ ,  $G\alpha_{q/412}$ ,  $G\alpha_{q/413}$ ,  $G\alpha_{q/414}$ ,  $G\alpha_{q/415}$ ,  $G\alpha_{q/416}$ ,  $G\alpha_{q/417}$ ,  $G\alpha_{q/418}$ ,  $G\alpha_{q/419}$ ,  $G\alpha_{q/420}$ ,  $G\alpha_{q/421}$ ,  $G\alpha_{q/422}$ ,  $G\alpha_{q/423}$ ,  $G\alpha_{q/424}$ ,  $G\alpha_{q/425}$ ,  $G\alpha_{q/426}$ ,  $G\alpha_{q/427}$ ,  $G\alpha_{q/428}$ ,  $G\alpha_{q/429}$ ,  $G\alpha_{q/430}$ ,  $G\alpha_{q/431}$ ,  $G\alpha_{q/432}$ ,  $G\alpha_{q/433}$ ,  $G\alpha_{q/434}$ ,  $G\alpha_{q/435}$ ,  $G\alpha_{q/436}$ ,  $G\alpha_{q/437}$ ,  $G\alpha_{q/438}$ ,  $G\alpha_{q/439}$ ,  $G\alpha_{q/440}$ ,  $G\alpha_{q/441}$ ,  $G\alpha_{q/442}$ ,  $G\alpha_{q/443}$ ,  $G\alpha_{q/444}$ ,  $G\alpha_{q/445}$ ,  $G\alpha_{q/446}$ ,  $G\alpha_{q/447}$ ,  $G\alpha_{q/448}$ ,  $G\alpha_{q/449}$ ,  $G\alpha_{q/450}$ ,  $G\alpha_{q/451}$ ,  $G\alpha_{q/452}$ ,  $G\alpha_{q/453}$ ,  $G\alpha_{q/454}$ ,  $G\alpha_{q/455}$ ,  $G\alpha_{q/456}$ ,  $G\alpha_{q/457}$ ,  $G\alpha_{q/458}$ ,  $G\alpha_{q/459}$ ,  $G\alpha_{q/460}$ ,  $G\alpha_{q/461}$ ,  $G\alpha_{q/462}$ ,  $G\alpha_{q/463}$ ,  $G\alpha_{q/464}$ ,  $G\alpha_{q/465}$ ,  $G\alpha_{q/466}$ ,  $G\alpha_{q/467}$ ,  $G\alpha_{q/468}$ ,  $G\alpha_{q/469}$ ,  $G\alpha_{q/470}$ ,  $G\alpha_{q/471}$ ,  $G\alpha_{q/472}$ ,  $G\alpha_{q/473}$ ,  $G\alpha_{q/474}$ ,  $G\alpha_{q/475}$ ,  $G\alpha_{q/476}$ ,  $G\alpha_{q/477}$ ,  $G\alpha_{q/478}$ ,  $G\alpha_{q/479}$ ,  $G\alpha_{q/480}$ ,  $G\alpha_{q/481}$ ,  $G\alpha_{q/482}$ ,  $G\alpha_{q/483}$ ,  $G\alpha_{q/484}$ ,  $G\alpha_{q/485}$ ,  $G\alpha_{q/486}$ ,  $G\alpha_{q/487}$ ,  $G\alpha_{q/488}$ ,  $G\alpha_{q/489}$ ,  $G\alpha_{q/490}$ ,  $G\alpha_{q/491}$ ,  $G\alpha_{q/492}$ ,  $G\alpha_{q/493}$ ,  $G\alpha_{q/494}$ ,  $G\alpha_{q/495}$ ,  $G\alpha_{q/496}$ ,  $G\alpha_{q/497}$ ,  $G\alpha_{q/498}$ ,  $G\alpha_{q/499}$ ,  $G\alpha_{q/500}$ ,  $G\alpha_{q/501}$ ,  $G\alpha_{q/502}$ ,  $G\alpha_{q/503}$ ,  $G\alpha_{q/504}$ ,  $G\alpha_{q/505}$ ,  $G\alpha_{q/506}$ ,  $G\alpha_{q/507}$ ,  $G\alpha_{q/508}$ ,  $G\alpha_{q/509}$ ,  $G\alpha_{q/510}$ ,  $G\alpha_{q/511}$ ,  $G\alpha_{q/512}$ ,  $G\alpha_{q/513}$ ,  $G\alpha_{q/514}$ ,  $G\alpha_{q/515}$ ,  $G\alpha_{q/516}$ ,  $G\alpha_{q/517}$ ,  $G\alpha_{q/518}$ ,  $G\alpha_{q/519}$ ,  $G\alpha_{q/520}$ ,  $G\alpha_{q/521}$ ,  $G\alpha_{q/522}$ ,  $G\alpha_{q/523}$ ,  $G\alpha_{q/524}$ ,  $G\alpha_{q/525}$ ,  $G\alpha_{q/526}$ ,  $G\alpha_{q/527}$ ,  $G\alpha_{q/528}$ ,  $G\alpha_{q/529}$ ,  $G\alpha_{q/530}$ ,  $G\alpha_{q/531}$ ,  $G\alpha_{q/532}$ ,  $G\alpha_{q/533}$ ,  $G\alpha_{q/534}$ ,  $G\alpha_{q/535}$ ,  $G\alpha_{q/536}$ ,  $G\alpha_{q/537}$ ,  $G\alpha_{q/538}$ ,  $G\alpha_{q/539}$ ,  $G\alpha_{q/540}$ ,  $G\alpha_{q/541}$ ,  $G\alpha_{q/542}$ ,  $G\alpha_{q/543}$ ,  $G\alpha_{q/544}$ ,  $G\alpha_{q/545}$ ,  $G\alpha_{q/546}$ ,  $G\alpha_{q/547}$ ,  $G\alpha_{q/548}$ ,  $G\alpha_{q/549}$ ,  $G\alpha_{q/550}$ ,  $G\alpha_{q/551}$ ,  $G\alpha_{q/552}$ ,  $G\alpha_{q/553}$ ,  $G\alpha_{q/554}$ ,  $G\alpha_{q/555}$ ,  $G\alpha_{q/556}$ ,  $G\alpha_{q/557}$ ,  $G\alpha_{q/558}$ ,  $G\alpha_{q/559}$ ,  $G\alpha_{q/560}$ ,  $G\alpha_{q/561}$ ,  $G\alpha_{q/562}$ ,  $G\alpha_{q/563}$ ,  $G\alpha_{q/564}$ ,  $G\alpha_{q/565}$ ,  $G\alpha_{q/566}$ ,  $G\alpha_{q/567}$ ,  $G\alpha_{q/568}$ ,  $G\alpha_{q/569}$ ,  $G\alpha_{q/570}$ ,  $G\alpha_{q/571}$ ,  $G\alpha_{q/572}$ ,  $G\alpha_{q/573}$ ,  $G\alpha_{q/574}$ ,  $G\alpha_{q/575}$ ,  $G\alpha_{q/576}$ ,  $G\alpha_{q/577}$ ,  $G\alpha_{q/578}$ ,  $G\alpha_{q/579}$ ,  $G\alpha_{q/580}$ ,  $G\alpha_{q/581}$ ,  $G\alpha_{q/582}$ ,  $G\alpha_{q/583}$ ,  $G\alpha_{q/584}$ ,  $G\alpha_{q/585}$ ,  $G\alpha_{q/586}$ ,  $G\alpha_{q/587}$ ,  $G\alpha_{q/588}$ ,  $G\alpha_{q/589}$ ,  $G\alpha_{q/590}$ ,  $G\alpha_{q/591}$ ,  $G\alpha_{q/592}$ ,  $G\alpha_{q/593}$ ,  $G\alpha_{q/594}$ ,  $G\alpha_{q/595}$ ,  $G\alpha_{q/596}$ ,  $G\alpha_{q/597}$ ,  $G\alpha_{q/598}$ ,  $G\alpha_{q/599}$ ,  $G\alpha_{q/600}$ ,  $G\alpha_{q/601}$ ,  $G\alpha_{q/602}$ ,  $G\alpha_{q/603}$ ,  $G\alpha_{q/604}$ ,  $G\alpha_{q/605}$ ,  $G\alpha_{q/606}$ ,  $G\alpha_{q/607}$ ,  $G\alpha_{q/608}$ ,  $G\alpha_{q/609}$ ,  $G\alpha_{q/610}$ ,  $G\alpha_{q/611}$ ,  $G\alpha_{q/612}$ ,  $G\alpha_{q/613}$ ,  $G\alpha_{q/614}$ ,  $G\alpha_{q/615}$ ,  $G\alpha_{q/616}$ ,  $G\alpha_{q/617}$ ,  $G\alpha_{q/618}$ ,  $G\alpha_{q/619}$ ,  $G\alpha_{q/620}$ ,  $G\alpha_{q/621}$ ,  $G\alpha_{q/622}$ ,  $G\alpha_{q/623}$ ,  $G\alpha_{q/624}$ ,  $G\alpha_{q/625}$ ,  $G\alpha_{q/626}$ ,  $G\alpha_{q/627}$ ,  $G\alpha_{q/628}$ ,  $G\alpha_{q/629}$ ,  $G\alpha_{q/630}$ ,  $G\alpha_{q/631}$ ,  $G\alpha_{q/632}$ ,  $G\alpha_{q/633}$ ,  $G\alpha_{q/634}$ ,  $G\alpha_{q/635}$ ,  $G\alpha_{q/636}$ ,  $G\alpha_{q/637}$ ,  $G\alpha_{q/638}$ ,  $G\alpha_{q/639}$ ,  $G\alpha_{q/640}$ ,  $G\alpha_{q/641}$ ,  $G\alpha_{q/642}$ ,  $G\alpha_{q/643}$ ,  $G\alpha_{q/644}$ ,  $G\alpha_{q/645}$ ,  $G\alpha_{q/646}$ ,  $G\alpha_{q/647}$ ,  $G\alpha_{q/648}$ ,  $G\alpha_{q/649}$ ,  $G\alpha_{q/650}$ ,  $G\alpha_{q/651}$ ,  $G\alpha_{q/652}$ ,  $G\alpha_{q/653}$ ,  $G\alpha_{q/654}$ ,  $G\alpha_{q/655}$ ,  $G\alpha_{q/656}$ ,  $G\alpha_{q/657}$ ,  $G\alpha_{q/658}$ ,  $G\alpha_{q/659}$ ,  $G\alpha_{q/660}$ ,  $G\alpha_{q/661}$ ,  $G\alpha_{q/662}$ ,  $G\alpha_{q/663}$ ,  $G\alpha_{q/664}$ ,  $G\alpha_{q/665}$ ,  $G\alpha_{q/666}$ ,  $G\alpha_{q/667}$ ,  $G\alpha_{q/668}$ ,  $G\alpha_{q/669}$ ,  $G\alpha_{q/670}$ ,  $G\alpha_{q/671}$ ,  $G\alpha_{q/672}$ ,  $G\alpha_{q/673}$ ,  $G\alpha_{q/674}$ ,  $G\alpha_{q/675}$ ,  $G\alpha_{q/676}$ ,  $G\alpha_{q/677}$ ,  $G\alpha_{q/678}$ ,  $G\alpha_{q/679}$ ,  $G\alpha_{q/680}$ ,  $G\alpha_{q/681}$ ,  $G\alpha_{q/682}$ ,  $G\alpha_{q/683}$ ,  $G\alpha_{q/684}$ ,  $G\alpha_{q/685}$ ,  $G\alpha_{q/686}$ ,  $G\alpha_{q/687}$ ,  $G\alpha_{q/688}$ ,  $G\alpha_{q/689}$ ,  $G\alpha_{q/690}$ ,  $G\alpha_{q/691}$ ,  $G\alpha_{q/692}$ ,  $G\alpha_{q/693}$ ,  $G\alpha_{q/694}$ ,  $G\alpha_{q/695}$ ,  $G\alpha_{q/696}$ ,  $G\alpha_{q/697}$ ,  $G\alpha_{q/698}$ ,  $G\alpha_{q/699}$ ,  $G\alpha_{q/700}$ ,  $G\alpha_{q/701}$ ,  $G\alpha_{q/702}$ ,  $G\alpha_{q/703}$ ,  $G\alpha_{q/704}$ ,  $G\alpha_{q/705}$ ,  $G\alpha_{q/706}$ ,  $G\alpha_{q/707}$ ,  $G\alpha_{q/708}$ ,  $G\alpha_{q/709}$ ,  $G\alpha_{q/710}$ ,  $G\alpha_{q/711}$ ,  $G\alpha_{q/712}$ ,  $G\alpha_{q/713}$ ,  $G\alpha_{q/714}$ ,  $G\alpha_{q/715}$ ,  $G\alpha_{q/716}$ ,  $G\alpha_{q/717}$ ,  $G\alpha_{q/718}$ ,  $G\alpha_{q/719}$ ,  $G\alpha_{q/720}$ ,  $G\alpha_{q/721}$ ,  $G\alpha_{q/722}$ ,  $G\alpha_{q/723}$ ,  $G\alpha_{q/724}$ ,  $G\alpha_{q/725}$ ,  $G\alpha_{q/726}$ ,  $G\alpha_{q/727}$ ,  $G\alpha_{q/728}$ ,  $G\alpha_{q/729}$ ,  $G\alpha_{q/730}$ ,  $G\alpha_{q/731}$ ,  $G\alpha_{q/732}$ ,  $G\alpha_{q/733}$ ,  $G\alpha_{q/734}$ ,  $G\alpha_{q/735}$ ,  $G\alpha_{q/736}$ ,  $G\alpha_{q/737}$ ,  $G\alpha_{q/738}$ ,  $G\alpha_{q/739}$ ,  $G\alpha_{q/740}$ ,  $G\alpha_{q/741}$ ,  $G\alpha_{q/742}$ ,  $G\alpha_{q/743}$ ,  $G\alpha_{q/744}$ ,  $G\alpha_{q/745}$ ,  $G\alpha_{q/746}$ ,  $G\alpha_{q/747}$ ,  $G\alpha_{q/748}$ ,  $G\alpha_{q/749}$ ,  $G\alpha_{q/750}$ ,  $G\alpha_{q/751}$ ,  $G\alpha_{q/752}$ ,  $G\alpha_{q/753}$ ,  $G\alpha_{q/754}$ ,  $G\alpha_{q/755}$ ,  $G\alpha_{q/756}$ ,  $G\alpha_{q/757}$ ,  $G\alpha_{q/758}$ ,  $G\alpha_{q/759}$ ,  $G\alpha_{q/760}$ ,  $G\alpha_{q/761}$ ,  $G\alpha_{q/762}$ ,  $G\alpha_{q/763}$ ,  $G\alpha_{q/764}$ ,  $G\alpha_{q/765}$ ,  $G\alpha_{q/766}$ ,  $G\alpha_{q/767}$ ,  $G\alpha_{q/768}$ ,  $G\alpha_{q/769}$ ,  $G\alpha_{q/770}$ ,  $G\alpha_{q/771}$ ,  $G\alpha_{q/772}$ ,  $G\alpha_{q/773}$ ,  $G\alpha_{q/774}$ ,  $G\alpha_{q/775}$ ,  $G\alpha_{q/776}$ ,  $G\alpha_{q/777}$ ,  $G\alpha_{q/778}$ ,  $G\alpha_{q/779}$ ,  $G\alpha_{q/780}$ ,  $G\alpha_{q/781}$ ,  $G\alpha_{q/782}$ ,  $G\alpha_{q/783}$ ,  $G\alpha_{q/784}$ ,  $G\alpha_{q/785}$ ,  $G\alpha_{q/786}$ ,  $G\alpha_{q/787}$ ,  $G\alpha_{q/788}$ ,  $G\alpha_{q/789}$ ,  $G\alpha_{q/790}$ ,  $G\alpha_{q/791}$ ,  $G\alpha_{q/792}$ ,  $G\alpha_{q/793}$ ,  $G\alpha_{q/794}$ ,  $G\alpha_{q/795}$ ,  $G\alpha_{q/796}$ ,  $G\alpha_{q/797}$ ,  $G\alpha_{q/798}$ ,  $G\alpha_{q/799}$ ,  $G\alpha_{q/800}$ ,  $G\alpha_{q/801}$ ,  $G\alpha_{q/802}$ ,  $G\alpha_{q/803}$ ,  $G\alpha_{q/804}$ ,  $G\alpha_{q/805}$ ,  $G\alpha_{q/806}$ ,  $G\alpha_{q/807}$ ,  $G\alpha_{q/808}$ ,  $G\alpha_{q/809}$ ,  $G\alpha_{q/810}$ ,  $G\alpha_{q/811}$ ,  $G\alpha_{q/812}$ ,  $G\alpha_{q/813$

were purchased from Japan Clea, and RNA was isolated from multiple tissues. RNA samples were reverse-transcribed into cDNA and were subjected to qPCR analysis. The primers used for the relative quantification are shown in Supplementary Data 4. The expression levels of hUTS2R and mUTS2R were normalized to housekeeping genes of G3PDH and 18 s rRNA, respectively.

#### Cell culture of human induced pluripotent stem cell-derived cardiomyocytes.

Human induced pluripotent stem cell-derived cardiomyocytes (hiPSC-CMs) were purchased from Fujifilm Cellular Dynamics, Inc. (CDI; iCell cardiomyocytes 2.0). To prepare the probe (MED-PG515A, Alpha MED Sciences), the recording areas were coated with fibronectin and dissolved in Dulbecco's phosphate-buffered saline to create a 50 µg/mL solution. The recording area was covered with 1–2 µL fibronectin solution, and the probes were incubated at 37 °C for at least 1 h. Cells were thawed and suspended in iCell Cardiomyocytes Plating Medium (CDI) and plated onto the probes at a density of  $3.5 \times 10^4$  cells in a 2 µL plating medium. The cells were incubated at 37 °C in 5% CO<sub>2</sub> for 3–4 h before filling each probe with 1 mL iCell cardiomyocytes maintenance medium (CDI), which was used as the culture medium. The medium was changed every 2–3 days, with the cells cultured in the probes for 5–14 days to obtain a sheet of cardiomyocytes with spontaneous and synchronous electrical activity.

**FP recordings and data analysis.** FP recording was carried out<sup>35,60</sup>. Before measuring FPs, iCell cardiomyocyte sheets were equilibrated for at least 4 h in a fresh culture medium using a 5% CO<sub>2</sub> incubator at 37 °C. After equilibration, the probes were transferred to the multi-electrode array (MEA) system (MED64, Alpha med Scientific) and incubated in a humidified 5% CO<sub>2</sub> atmosphere. The stability and constancy of the waveforms were confirmed by monitoring the signals for at least 30 min. Once the FPs reached a stable state, they were recorded for 10 min at the baseline and then 24, 48, and 72 h after drug treatment. The stock solutions of drugs were prepared in dimethyl sulfoxide (DMSO) or distilled water at a 1000-fold target concentration. The stock solution was diluted in a culture medium to a final concentration of 0.1% DMSO.

The FP duration (FPD) was defined as the duration from the first to the second peak in FP<sup>35</sup>. The FPD was corrected for the beat rate (inter-spike interval (ISI)) with Fridericia's formula (Eq. 1), which was the primary method of correction in this study:

$$(\text{FPDcF} = \text{FPD}/(\text{ISI}/1000)^{1/3}). \quad (1)$$

The ISI and FPD values were averaged from the last 30 beats or 30 beats at time points exhibiting a stable ISI and FPD.

**Patch-clamp technique using hiPS-CMs.** The perforated patch-clamp technique was used to record spontaneous action potentials in current-clamp models of hiPS-CMs at 25 °C, using an EPC-10 patch-clamp amplifier (HEKA, Lambrecht, Germany)<sup>61</sup>. The hiPS-CMs typically generate spontaneous automaticity in normal Tyrode solution. Spontaneous action potentials were recorded using a fire-polished patch pipette (resistance, 2.0–4.0 MΩ) filled with a pipette solution containing 70 mM potassium aspartate, 50 mM KCl, 10 mM KH<sub>2</sub>PO<sub>4</sub>, 1 mM MgSO<sub>4</sub>, 3 mM adenosine triphosphate (ATP) (disodium salt; Sigma Chemical Company, St Louis), 5 mM EGTA, 5 mM HEPES, and 0.1 mM Li<sub>2</sub>-guanosine triphosphate (GTP) (Sigma Chemical Company) (pH adjusted to 7.2 with KOH). Amphotericin B (Wako Pure Chemical Industries) was added to the pipette solution at a concentration of 100 mg/mL. The glass coverslip (3 × 5 mm<sup>2</sup>) containing hiPS-CMs plated in 35-mm culture dishes was placed into a recording chamber with normal Tyrode solution.<sup>62</sup>

#### Isolation of neonatal rat cardiomyocyte.

Neonatal rat cardiomyocytes (NRCMs) were isolated from Sprague-Dawley rat (Japan SLC Inc.) pups on postnatal days 1–3<sup>62</sup>. The ventricles of the pups were dissected and minced on ice after terminal anesthesia (1.5% sevoflurane inhalation) and euthanasia by cervical dislocation. The minced tissue was pre-digested in 0.05% trypsin-EDTA (Gibco) overnight at 4 °C and then digested in 1 mg/mL collagenase type2 (Worthington) in PBS for 30 min at 37 °C while shaking the flask (125 rpm). The dissociated cells were filtered through a cell strainer (70 µm, Falcon) and centrifuged for 2 min at 180×g. After removing the supernatant, cell pellets were resuspended in Dulbecco's modified Eagle's medium 12 (DMEM) supplemented with 10% FBS and 1% penicillin and streptomycin plated in a 10-cm culture dish. Cells were incubated at 37 °C in a humidified atmosphere (5% CO<sub>2</sub>, 95% air) for 90 min. Floating NRCMs were collected and plated to matrigel-coated culture dishes. After 24 h, the culture medium was changed to serum-free DMEM and incubated for more than 2 days before experiments. All animal experiments were reviewed and approved by the ethics committees at the National Institutes of Natural Sciences or the Animal Care and Use Committee at Kyushu University. All reported procedures conform to the NIH Guide for the Care and Use of Laboratory Animals.

**Observation and analysis of contractility with pacing.** NRCMs ( $4 \times 10^5$  cells/well) were seeded on 3.5-cm glass-bottomed dishes in serum-free DMEM. Cells were treated with remdesivir (1 µM) for 48 h at 37 °C and 5%CO<sub>2</sub>. Urantide (100 nM) was added at the same time. Pertussis toxin (PTX; 150 ng/mL) was treated 18 h before

adding remdesivir, and YM-254890 (1 µM) was treated 30 minutes before remdesivir addition. Microscopic images of NRCMs were recorded for 13 s under pacing conditions. The pacing of NRCM was stimulated at 4 V every second, with a frequency of 10 ms, using an electrical stimulator (NIHON KOHDEN, SEN-3301). Imaging data were acquired at six frames per second using a BZ-X800 microscope (Keyence) and analyzed using Fiji software<sup>63</sup>.

#### Isolation of adult mouse cardiomyocyte.

C57BL/6J mice for the isolation of adult mouse cardiomyocytes were purchased from Japan SLC Inc. (Shizuoka, Japan). Isolation of adult mouse ventricular cardiomyocytes was performed<sup>64</sup>. Male mice were anesthetized by inhalation with isoflurane. The heart was quickly excised, and the aorta was clamped with a small vascular clamp. The heart was antegradely perfused with isolation buffer (less than 3 mL) containing 130 mM NaCl, 5.4 mM KCl, 0.5 mM MgCl<sub>2</sub>, 0.33 mM NaH<sub>2</sub>PO<sub>4</sub>, 25 mM HEPES, 22 mM glucose, and 50 µU/mL bovine insulin (Sigma) (pH 7.4, adjusted with NaOH) supplemented with 0.4 mM EGTA, followed by the perfusion of enzyme solution (10 mL) (isolation buffer containing 1 mg/mL collagenase type 2 (Worthington), 0.06 mg/mL trypsin (Sigma), 0.06 mg/mL protease (Sigma), and 0.3 mM CaCl<sub>2</sub>). Thereafter, the LV chamber was removed and cut into small pieces in an enzyme solution containing 0.2% bovine serum albumin (BSA) and 0.7 mM CaCl<sub>2</sub>. The tissue-cell suspension was filtered through a cell strainer (100 µm, Falcon) and centrifuged for 3 min at 50×g. After removing the supernatant, the cell pellet was resuspended in isolation buffer supplemented with 0.2% BSA and 1.2 mM CaCl<sub>2</sub> and incubated for 7 min at 37 °C. After centrifugation (50×g, 3 min), the cells were resuspended in Tyrode's solution A (containing 140 mM NaCl, 5.4 mM KCl, 1.8 mM CaCl<sub>2</sub>, 0.5 mM MgCl<sub>2</sub>, 0.33 mM NaH<sub>2</sub>PO<sub>4</sub>, 5.0 mM HEPES, and 5.5 mM glucose (pH 7.4)) supplemented with 0.2% BSA. Cells were seeded onto Matrigel (Corning)-coated 35 mm glass base dishes (IWAKI) and incubated at 37 °C for 30 min. Cells were used within 1–6 h after isolation.

#### Observation of contractility with the pacing of adult mouse cardiomyocytes.

Isolated adult mouse cardiomyocytes were treated with remdesivir (10 µM) for 30 min at 37 °C. Microscopic images of cardiomyocytes were recorded for 13 seconds under pacing conditions. The pacing of cardiomyocytes was stimulated at 30 V every second with a frequency of 10 msec using an electrical stimulator (NIHON KOHDEN, SEN-3301). Imaging data were analyzed using Fiji software.

**Statistics and reproducibility.** Statistical analyses were performed with Prism Software (GraphPad), and methods are described in the figure legends. Symbols are mean values, and error bars denote the standard error of the mean (SEM). Representative results from at least three independent experiments are shown for every figure unless stated otherwise in the figure legends.

**Reporting summary.** Further information on research design is available in the Nature Portfolio Reporting Summary linked to this article.

#### Data availability

All data are available in the main text or the supplementary materials. Source data underlying figures are provided in Supplementary Data 1. Uncropped blots are presented in Supplementary Fig. 5. Molecular docking simulation files were deposited to [Zenodo](https://zenodo.org/).

Received: 10 November 2022; Accepted: 28 April 2023;

Published online: 12 May 2023

#### References

- Seley-Radtke, K. L. & Yates, M. K. The evolution of nucleoside analogue antivirals: a review for chemists and non-chemists. Part 1: early structural modifications to the nucleoside scaffold. *Antiviral Res.* **154**, 66–86 (2018).
- Chien, M. et al. Nucleotide analogues as inhibitors of SARS-CoV-2 polymerase, a key drug target for COVID-19. *J. Proteome Res.* **19**, 4690–4697 (2020).
- Alanazi, A. S., James, E. & Mehellou, Y. The ProTide prodrug technology: where next? *ACS Med. Chem. Lett.* **10**, 2–5 (2019).
- Sheahan, T. P. et al. Broad-spectrum antiviral GS-5734 inhibits both epidemic and zoonotic coronaviruses. *Sci. Transl. Med.* **9**, eaal3653 (2017).
- Siegel, D. et al. Discovery and synthesis of a phosphoramidate prodrug of a Pyrrolo[2,1-f][triazin-4-amino] adenine C-nucleoside (GS-5734) for the treatment of Ebola and emerging viruses. *J. Med. Chem.* **60**, 1648–1661 (2017).
- Warren, T. K. et al. Therapeutic efficacy of the small molecule GS-5734 against Ebola virus in rhesus monkeys. *Nature* **531**, 381–385 (2016).
- Beigel, J. H. et al. Remdesivir for the treatment of Covid-19—final report. *N. Engl. J. Med.* **383**, 1813–1826 (2020).

8. Gottlieb, R. L. et al. Early remdesivir to prevent progression to severe Covid-19 in outpatients. *N. Engl. J. Med.* **386**, 305–315 (2022).
9. Coronavirus Disease 2019 (COVID-19) Treatment Guidelines. (2022).
10. Jung, S. Y. et al. Cardiovascular events and safety outcomes associated with remdesivir using a World Health Organization international pharmacovigilance database. *Clin. Transl. Sci.* **15**, 501–513 (2022).
11. Haghjoo, M. et al. Effect of COVID-19 medications on corrected QT interval and induction of torsade de pointes: Results of a multicenter national survey. *Int. J. Clin. Pract.* **75**, e14182 (2021).
12. Liu, D. et al. Adverse cardiovascular effects of anti-COVID-19 drugs. *Front. Pharmacol.* **12**, 699949 (2021).
13. Gupta, A. K., Parker, B. M., Priyadarshi, V. & Parker, J. Cardiac adverse events with remdesivir in COVID-19 infection. *Cureus* **12**, e11132 (2020).
14. Hu, W. J. et al. Pharmacokinetics and tissue distribution of remdesivir and its metabolites nucleotide monophosphate, nucleotide triphosphate, and nucleoside in mice. *Acta Pharmacol. Sin.* **42**, 1195–1200 (2021).
15. Gordon, C. J., Tchesnokov, E. P., Schinazi, R. F. & Götte, M. Molnupiravir promotes SARS-CoV-2 mutagenesis via the RNA template. *J. Biol. Chem.* **297**, 100770 (2021).
16. Jayk Bernal, A. et al. Molnupiravir for oral treatment of Covid-19 in nonhospitalized patients. *N. Engl. J. Med.* **386**, 509–520 (2022).
17. Furuta, Y. et al. T-705 (favipiravir) and related compounds: Novel broad-spectrum inhibitors of RNA viral infections. *Antiviral Res.* **82**, 95–102 (2009).
18. Padhi, A. K., Dandapat, J., Saudagar, P., Uversky, V. N. & Tripathi, T. Interface-based design of the favipiravir-binding site in SARS-CoV-2 RNA-dependent RNA polymerase reveals mutations conferring resistance to chain termination. *FEBS Lett.* **595**, 2366–2382 (2021).
19. Wen, W. et al. Efficacy and safety of three new oral antiviral treatment (molnupiravir, fluvoxamine and Paxlovid) for COVID-19: a meta-analysis. *Ann. Med.* **54**, 516–523 (2022).
20. Hung, D. T. et al. The efficacy and adverse effects of favipiravir on patients with COVID-19: a systematic review and meta-analysis of published clinical trials and observational studies. *Int. J. Infect. Dis.* **120**, 217–227 (2022).
21. Jacobson, K. A. & Gao, Z. G. Adenosine receptors as therapeutic targets. *Nat Rev Drug Discov* **5**, 247–264 (2006).
22. Ogawa, A. et al. N(6)-methyladenosine (m(6)A) is an endogenous A3 adenosine receptor ligand. *Mol. Cell* **81**, 659–674.e657 (2021).
23. Rengo, G., Lymperopoulos, A. & Koch, W. J. Future g protein-coupled receptor targets for treatment of heart failure. *Curr. Treat. Options Cardiovasc. Med.* **11**, 328–338 (2009).
24. Sato, M. & Ishikawa, Y. Accessory proteins for heterotrimeric G-protein: implication in the cardiovascular system. *Pathophysiology* **17**, 89–99 (2010).
25. Wacker, D., Stevens, R. C. & Roth, B. L. How ligands illuminate GPCR molecular pharmacology. *Cell* **170**, 414–427 (2017).
26. Inoue, A. et al. TGF $\alpha$  shedding assay: an accurate and versatile method for detecting GPCR activation. *Nat. Methods* **9**, 1021–1029 (2012).
27. Summary-compassionate-use-remdesivir-gilead\_en.pdf. (2020).
28. Du, A. T. et al. Ligand-supported purification of the urotensin-II receptor. *Mol. Pharmacol.* **78**, 639–647 (2010).
29. Castel, H. et al. The G protein-coupled receptor UT of the neuropeptide urotensin II displays structural and functional chemokine features. *Front. Endocrinol.* **8**, 76 (2017).
30. Ballesteros, J. A. & Weinstein, I. Integrated methods for the construction of three-dimensional models and computational probing of structure-function relations in G protein-coupled receptors. *Methods Neurosci.* **25**, 366–428 (1995).
31. Biswal, H. S., Gloaguen, E., Loquais, Y., Tardivel, B. & Mons, M. Strength of NH $\cdots$ S hydrogen bonds in methionine residues revealed by gas-phase IR/UV spectroscopy. *J. Phys. Chem. Lett.* **3**, 755–759 (2012).
32. Pokkuluri, P. R. et al. Factors contributing to decreased protein stability when aspartic acid residues are in beta-sheet regions. *Protein Sci.* **11**, 1687–1694 (2002).
33. Pereira-Castro, J., Brás-Silva, C. & Fontes-Sousa, A. P. Novel insights into the role of urotensin II in cardiovascular disease. *Drug Discov. Today* **24**, 2170–2180 (2019).
34. Mummery, C. L. et al. Differentiation of human embryonic stem cells and induced pluripotent stem cells to cardiomyocytes: a methods overview. *Circ. Res.* **111**, 344–358 (2012).
35. Yanagida, S., Satsuka, A., Hayashi, S., Ono, A. & Kanda, Y. Comprehensive cardiotoxicity assessment of COVID-19 treatments using human-induced pluripotent stem cell-derived cardiomyocytes. *Toxicol. Sci.* **183**, 227–239 (2021).
36. Cubeddu, L. X. QT prolongation and fatal arrhythmias: a review of clinical implications and effects of drugs. *Am. J. Ther.* **10**, 452–457 (2003).
37. Wetschreck, N. & Offermanns, S. Mammalian G proteins and their cell type specific functions. *Physiol. Rev.* **85**, 1159–1204 (2005).
38. Nishida, M. et al. G $\alpha$ (i) and G $\alpha$ (o) are target proteins of reactive oxygen species. *Nature* **408**, 492–495 (2000).
39. Kwok, M. et al. Remdesivir induces persistent mitochondrial and structural damage in human induced pluripotent stem cell derived cardiomyocytes. *Cardiovasc. Res.* **118**, 2652–2664 (2022).
40. Tchesnokov, E. P., Feng, J. Y., Porter, D. P. & Götte, M. Mechanism of inhibition of Ebola virus RNA-dependent RNA polymerase by remdesivir. *Viruses* **11**, 326 (2019).
41. Tadaka, S. et al. jMorp updates in 2020: large enhancement of multi-omics data resources on the general Japanese population. *Nucleic Acids Res.* **49**, D536–d544 (2021).
42. Lasser, K. E. et al. Timing of new black box warnings and withdrawals for prescription medications. *J. Am. Med. Assoc.* **287**, 2215–2220 (2002).
43. Michaud, V. et al. Risk assessment of drug-induced long QT syndrome for some COVID-19 repurposed drugs. *Clin. Transl. Sci.* **14**, 20–28 (2021).
44. Nabati, M. & Parsaee, H. Potential cardiotoxic effects of remdesivir on cardiovascular system: a literature review. *Cardiovasc. Toxicol.* **22**, 268–272 (2022).
45. Day, L. B., Abdel-Qadir, H. & Fralick, M. Bradycardia associated with remdesivir therapy for COVID-19 in a 59-year-old man. *Can. Med. Assoc. J.* **193**, E612–e615 (2021).
46. Sanchez-Codez, M. I., Rodriguez-Gonzalez, M. & Gutierrez-Rosa, I. Severe sinus bradycardia associated with Remdesivir in a child with severe SARS-CoV-2 infection. *Eur. J. Pediatr.* **180**, 1627 (2021).
47. Douglas, S. A., Tayara, L., Ohlstein, E. H., Halawa, N. & Giaid, A. Congestive heart failure and expression of myocardial urotensin II. *Lancet* **359**, 1990–1997 (2002).
48. Adamsick, M. L. et al. Remdesivir in patients with acute or chronic kidney disease and COVID-19. *J. Am. Soc. Nephrol.* **31**, 1384–1386 (2020).
49. Insel, P. A., Tang, C. M., Hahntow, I. & Michel, M. C. Impact of GPCRs in clinical medicine: monogenic diseases, genetic variants and drug targets. *Biochim. Biophys. Acta* **1768**, 994–1005 (2007).
50. Lefkowitz, R. J. & Shenoy, S. K. Transduction of receptor signals by beta-arrestins. *Science* **308**, 512–517 (2005).
51. Esposito, G. et al. EGFR trans-activation by urotensin II receptor is mediated by  $\beta$ -arrestin recruitment and confers cardioprotection in pressure overload-induced cardiac hypertrophy. *Basic Res. Cardiol.* **106**, 577–589 (2011).
52. Korhonen, T., Hänninen, S. L. & Tavi, P. Model of excitation-contraction coupling of rat neonatal ventricular myocytes. *Biophys. J.* **96**, 1189–1209 (2009).
53. Sala, L. et al. MUSCLEMOTION: a versatile open software tool to quantify cardiomyocyte and cardiac muscle contraction in vitro and in vivo. *Circ Res.* **122**, e5–e16 (2018).
54. Sanguinetti, M. C. & Tristani-Firouzi, M. hERG potassium channels and cardiac arrhythmia. *Nature* **440**, 463–469 (2006).
55. Hisano, Y. et al. Lysolipid receptor cross-talk regulates lymphatic endothelial junctions in lymph nodes. *J. Exp. Med.* **216**, 1582–1598 (2019).
56. Jumper, J. et al. Highly accurate protein structure prediction with AlphaFold. *Nature* **596**, 583–589 (2021).
57. Varadi, M. et al. AlphaFold Protein Structure Database: massively expanding the structural coverage of protein-sequence space with high-accuracy models. *Nucleic Acids Res.* **50**, D439–d444 (2022).
58. Word, J. M., Lovell, S. C., Richardson, J. S. & Richardson, D. C. Asparagine and glutamine: using hydrogen atom contacts in the choice of side-chain amide orientation. *J. Mol. Biol.* **285**, 1735–1747 (1999).
59. Ravindranath, P. A., Forli, S., Goodsell, D. S., Olson, A. J. & Sanner, M. F. AutoDockFR: advances in protein-ligand docking with explicitly specified binding site flexibility. *PLoS Comput. Biol.* **11**, e1004586 (2015).
60. Ando, H. et al. A new paradigm for drug-induced torsadogenic risk assessment using human iPS cell-derived cardiomyocytes. *J. Pharmacol. Toxicol. Methods* **84**, 111–127 (2017).
61. Ding, W. G. et al. Identification of verapamil binding sites within human Kv1.5 channel using mutagenesis and docking simulation. *Cell Physiol. Biochem.* **52**, 302–314 (2019).
62. Kitajima, N. et al. TRPC3 positively regulates reactive oxygen species driving maladaptive cardiac remodeling. *Sci. Rep.* **6**, 37001 (2016).
63. Matsuda, Y., Takahashi, K., Kamioka, H. & Naruse, K. Human gingival fibroblast feeder cells promote maturation of induced pluripotent stem cells into cardiomyocytes. *Biochem. Biophys. Res. Commun.* **503**, 1798–1804 (2018).
64. Omatsu-Kanbe, M., Yoshioka, K., Fukunaga, R., Sagawa, H. & Matsuura, H. A simple antegrade perfusion method for isolating viable single cardiomyocytes from neonatal to aged mice. *Physiol. Rep.* **6**, e13688 (2018).

## Acknowledgements

We are grateful for suggestions and technical support from all members of the Department of Modomics Biology & Medicine, Tohoku University. We thank Y. Takahata and H. Miyamoto for technical assistance and Natalie D. DeWitt for critical reading and language editing. This work was supported by funding provided by JSPS KAKENHI (Grant nos. JP20K18371, JP22H04628, and JP22H02813 to A.O., JP21H05269 and JP22H02772 to M.N., JP21H04791 and JP21H051130 to A.I.,

JP21H02659 and JP21H05265 to F.Y.W., and JP21H02634 to Y. Kanda. This work was also supported by the AMED (Grant nos. JP21mk0101189 to Y. Kanda, JP22zf0127007 to A.I., 21he2302008j0002 to F.Y.W., BINDS JP22ama121031 to M.N. and JP20am0101095 to A.I., LEAP JP20gm0010004 to A.I.), FOREST from JST (Grant nos. JPMJFR220K to A.O., JPMJFR215T to A.I., JPMJFR205Y to F.Y.W.), Moonshot R&D JPMJMS2023 from JST to A.I., CREST JPMJCR2024 (20348438) from J.S.T. to M.N., ERATO JPMJER2002 from J.S.T. to F.Y.W., Daiichi Sankyo Foundation of Life Science to A.I., Takeda Science Foundation to A.O. and A.I., Uehara Memorial Foundation to A.O. and A.I., Inamori Foundation to A.O., the Mitsubishi Foundation to A.O., Terumo Life Science Foundation to A.O., and the Naito Foundation to A.O.

### Author contributions

The authors confirm their contribution to the paper as follows: study conceptualization and design: A.O., M.N., A.I., and F.Y.W.; data collection: A.O., S.O., Y. Kato, T.I., S.Y., X.M., Y.I., and A.I.; analysis and interpretation of results: A.O., Y. Kato, T.I., S.Y., X.M., Y. Kanda, M.N., A.I., and F.Y.W. draft paper preparation: A.O., Y. Kato, T.I., S.Y., X.M., A.I., F.Y.W. project supervision: Y. Kanda, M.N., A.I., F.Y.W. All authors reviewed the results and approved the final version of the paper.

### Competing interests

The authors declare no competing interests.

### Additional information

**Supplementary information** The online version contains supplementary material available at <https://doi.org/10.1038/s42003-023-04888-x>.

**Correspondence** and requests for materials should be addressed to Motohiro Nishida, Asuka Inoue or Fan-Yan Wei.

**Peer review information** *Communications Biology* thanks Dipayan Chaudhuri and the other anonymous reviewer(s) for their contribution to the peer review of this work. Primary Handling Editor: George Inglis.

**Reprints and permission information** is available at <http://www.nature.com/reprints>

**Publisher's note** Springer Nature remains neutral with regard to jurisdictional claims in published maps and institutional affiliations.



**Open Access** This article is licensed under a Creative Commons Attribution 4.0 International License, which permits use, sharing, adaptation, distribution and reproduction in any medium or format, as long as you give appropriate credit to the original author(s) and the source, provide a link to the Creative Commons license, and indicate if changes were made. The images or other third party material in this article are included in the article's Creative Commons license, unless indicated otherwise in a credit line to the material. If material is not included in the article's Creative Commons license and your intended use is not permitted by statutory regulation or exceeds the permitted use, you will need to obtain permission directly from the copyright holder. To view a copy of this license, visit <http://creativecommons.org/licenses/by/4.0/>.

© The Author(s) 2023